Castling, a novel therapeutic concept for rewiring pathological gene-expression networks, enabled by the TRIPLE technology

Dinu Antony[1,2,#], Maria Silvia Roman Azcona[1,2,#], Hagar Kalinski[3], Marianne Pultar[4], Swetlana Adamsky[3], Sharon Avkin Nachum[3], Eyal Shalom[3], Manuel Rhiel[1,2], Andreas Tsouris[5], Andreas Diendorfer[4], Geoffroy Andrieux[5,8], Melanie Boerries[5,6,7,8], Matthias Hackl[4], Tatjana I. Cornu[1,2,8], Daniel Zurr[3], Toni Cathomen[1,2,8], Elena Feinstein[3] and Claudio Mussolino[1,2,8,*].

[1]Institute for Transfusion Medicine and Gene Therapy, Medical Center – University of Freiburg, Freiburg, Germany

[2]Center for Cell and Gene Therapy Freiburg (CGF), Medical Center – University of Freiburg, Freiburg, Germany

[3]Lepton Pharmaceuticals LTD, Israel

[4]TAmiRNA GmbH, Vienna, Austria

[5]Institute of Medical Bioinformatics and Systems Medicine, Medical Center – University of Freiburg, Freiburg, Germany

[6]Comprehensive Cancer Center Freiburg (CCCF), Medical Center - University of Freiburg, Freiburg, Germany

[7]German Cancer Consortium (DKTK), Partner Site Freiburg, a partnership between DKFZ and Medical Center - University of Freiburg, Freiburg, Germany

[8]Faculty of Medicine, University of Freiburg, Freiburg, Germany

*Correspondence: claudio.mussolino@uniklinik-freiburg.de

[#]These two authors contributed equally.

Abstract

Background

Pathological conditions often arise from dysregulation of complex gene networks. MicroRNAs (miRNAs) are central modulators of these networks, with upregulation of "disease-promoting" miRNAs suppressing beneficial pathways, and downregulation of "protective/therapeutic" miRNAs normally restraining pathological programs. Because individual miRNAs coordinately regulate multiple genes, they represent powerful therapeutic targets. We hypothesized that pathology-associated gene expression imbalances could be corrected by placing downregulated "protective/therapeutic" miRNAs under the control of promoters driving overexpression of "disease-promoting" miRNAs, thereby simultaneously disabling pathogenic programs and inducing therapeutic ones. We termed this concept *castling*, after the chess move.

Methods

Candidate miRNA pairs for *castling* were identified as inversely regulated in CAR T cells at early and late stages of the chronic antigen stimulation eventually leading to their dysfunction. Proof-of-concept experiments with *castling* of selected miRNA clusters (knock in of miR-17~92 into a miR15/16 locus) was then implemented in both primary T cells and in CAR T cells using a newly developed genome-editing procedure TRIPLE (Targeted Replacement Induced by Persistent Locus Editing) that enhances homology-directed repair via sequential cleavage. This was followed by differential expression of miRNA and mRNAs resulting from *castling* compared to similarly treated non-*castled* corresponding control cells. In addition, *castled* CAR T cells were evaluated functionally in the chronic antigen stimulation assay.

Results

In primary T-cells, swapped expression patterns of the *castled* miR17~92 and miR15-16 clusters elicited expected bidirectional changes of expression of their predicted target mRNA subsets. In CAR T cells under chronic antigen stimulation, *castling* of these miRNA clusters delayed dysfunction, enhanced cytokine production, and reshaped transcriptional programs consistent with restored T cell fitness. This was accompanied by up- and downregulation of multiple supporting genes.

Conclusions

Castling, implemented via TRIPLE or any other suitable gene editing technology, offers a broadly applicable strategy to reprogram disease-driven gene regulatory networks by converting pathological regulatory loops into self-correcting circuits. As a conceptual therapeutic approach, *castling* may be broadly applicable for improvement of multiple types of cell therapies in a variety of indications as well as for manipulation of not only miRNA but also of protein coding mRNAs.

Keywords

Gene network modulation, Genome editing, MicroRNA regulation, CRISPR-Cas9, CAR T cell engineering

66 **Background**

67 The dysregulation of complex gene expression networks drives the development of many diseases and
68 pathological conditions, where coordinated changes in expression of multiple genes underlie dysfunctional
69 cellular states. In the early stages of disease, transient changes in transcription often represent adaptive
70 responses aimed at restoring homeostasis(1). However, as pathological stimuli persist, these regulatory
71 programs become increasingly distorted, leading to the sustained activation of genes that promote disease
72 progression and the repression of genes that maintain normal cellular function(2). MicroRNAs (miRNAs)
73 have emerged as central regulators in these dynamic transitions, acting as critical post-transcriptional
74 switches that fine-tune gene network activities with disease progression being frequently associated with
75 imbalance in miRNA expression. In this context, miRNAs that suppress pathways regulating cellular
76 integrity are progressively overexpressed, while those that inhibit disease-supportive pathways are
77 progressively silenced. For instance, miR-21-5p and miR-155-5p are consistently upregulated in cancer
78 and chronic inflammatory states(3-6), where they reinforce proliferation and pro-inflammatory signaling,
79 whereas miR-29a-3p, a key antifibrotic regulator, is repressed in tissue fibrosis, or miR-126-5p, essential
80 for vascular homeostasis, is downregulated in cardiovascular disease(7, 8). This coordinated dysregulation
81 contributes to the establishment of pathological gene expression programs that sustain disease and
82 suppress recovery. Since miRNAs naturally control the expression of multiple genes simultaneously, they
83 have emerged as attractive therapeutic targets for modulating complex gene circuits and the broader
84 signaling pathways they govern.

85 Existing approaches, such as miRNA mimetics to restore a protective miRNA exhibiting low expression or
86 antimirs to inhibit overexpressed pathogenic miRNAs, have shown conceptual promise(9-11) but still
87 suffer from several technical problems including poor physiological control(12, 13). For example, synthetic
88 miRNA mimetics or antimirs may act for durations that may not match the therapeutical need whereas,
89 overexpression of miRNA mimics or antimirs using, for example, gene therapy vectors may overwhelm the

endogenous miRNA processing machinery, leading to off-target effects and even cytotoxic outcomes(14, 15).

To overcome these limitations, we hypothesized that therapeutic restoration of normal cellular function in the context of pathology could be achieved by strategically rewiring miRNA regulation within the genome itself. Specifically, we reasoned that placing the sequence of an insufficiently expressed therapeutically beneficial miRNA under the control of a promoter that is activated under pathological conditions, would achieve two complementary goals: (i) high expression of the therapeutic miRNA during persistence of the pathological conditions, and (ii) disruption of the disease-promoting miRNA expression at that locus. This dual-action strategy would engage corrective regulatory mechanisms precisely during the pathological state, effectively using the disease's own transcriptional machinery against itself (**Figure 1a**). We termed this concept *castling*, after the strategic chess move that simultaneously repositions and protects key chess pieces on the board. Implementing *castling* required an advanced genome-editing strategy capable of performing precise sequence replacement at high efficiency. To this end, we developed TRIPLE (Targeted Replacement Induced by Persistent Locus Editing), a novel homology-directed repair–based approach that through recurrent cleavage, prolongs the repair time window at double-stranded breaks, markedly enhancing the frequency of precise insertion editing and enabling the reliable execution of *castling*.

Here we demonstrate that *castling* can be used to rewire a pathogenic miRNA regulatory network into a configuration that sustains cellular function. For the proof of *castling* concept, we used an *in vitro* model of CAR T cell dysfunction which is progressively induced by chronic antigen stimulation. This model reproduces, at least in part, a known T cell exhaustion phenotype, a dysfunctional state characterized by diminished effector function, sustained expression of inhibitory receptors, restricted proliferative capacity and altered transcriptional programs(16, 17). Notably, in the clinics, engineered CAR T cells also acquire an exhausted phenotype upon entering the tumor microenvironment where they are exposed to target

114 tumor antigens and tumor-derived inhibitory factors, underscoring that CAR T cell exhaustion is a major
115 barrier to their durable therapeutic efficacy(18, 19). In line with this, several therapeutic strategies aim to
116 mitigate exhaustion, for example, by blocking checkpoint receptor–ligand interactions through antibodies
117 or gene-editing approaches, thereby delaying the dysfunction onset(20, 21). We first conducted a time-
118 resolved analysis of miRNA expression in this model and identified inversely regulated miRNA pairs whose
119 temporal expression patterns suggested opposing roles in promoting versus counteracting CAR T cells
120 dysfunction. Guided by these findings, we employed TRIPLE to efficiently replace disease-promoting
121 miRNAs, at their endogenous loci, with sequences of protective miRNA counterparts. This intervention
122 reactivated gene expression programs associated with sustained effector function and prolonged cytotoxic
123 activity while disabling the inhibitory programs, collectively translating into a measurable delay in the
124 onset of CAR T cell dysfunction.

125 Together, our findings establish *castling* as a versatile approach for disease-responsive genome
126 reprogramming and TRIPLE as its enabling technology. This work lays the foundation for the development
127 of a next-generation therapeutic platform in which disease-associated regulatory networks can be
128 precisely rewired at the genomic level to sustain cellular health and combat complex pathologies.

129

130 **Methods**

131 **Cell lines and primary T cell culture conditions**

132 Peripheral blood mononuclear cells (PBMCs) from healthy donors were obtained from leukoreduction
133 system (LRS) chambers and isolated by density gradient centrifugation using Biocoll (Bio&SELL,
134 Nuremberg, Germany). Primary T cells were obtained from PBMCs either by enrichment after activation
135 or by negative selection using the EasySep™ Human T Cell Isolation Kit (Stemcell Technologies, Vancouver,
136 Canada) to yield a pure $CD3^+$ cell population. T cells or CAR T cells were cultured in complete RPMI medium

137 consisting of RPMI 1640 GlutaMAX (Life Technologies, Carlsbad, CA), 10% FBS (PAN Biotech, Aidenbach,
138 Germany), 1X penicillin–streptomycin, and 10 mM HEPES buffer (Sigma-Aldrich, St. Louis, MO). Unless
139 stated otherwise, this medium was supplemented with 100 U/mL recombinant human IL-2 (rhIL-2;
140 ImmunoTools, Friesoythe, Germany). Medium was replaced every 2–3 days depending on the rate of cell
141 expansion. NALM6 cells naturally expressing the CD19 antigen were transduced with a lentivirus to express
142 GFP (NALM6-GFP$^+$), as described previously(17), and cultured in the same medium as T cells but without
143 rhIL-2 supplementation. All cells were maintained at 37 °C in a humidified atmosphere containing 5% CO_2.

144 **T cell manipulation**

145 Primary T cells (from PBMCs or isolated CD3$^+$ cells) were activated in activation medium consisting of
146 complete RPMI supplemented with ImmunoCult™ Human CD3/CD28/CD2 T Cell Activator (Stemcell
147 Technologies, Vancouver, Canada) at a final concentration of 10 µL/mL and rhIL-2 at 100 U/mL. Cell density
148 was kept at $2x10^6$ cells/mL. Afterwards, T cells were either subjected to *castling* via genome editing or
149 first transduced to express a CD19-specific CAR prior *castling*. For the genome editing procedure, activated
150 T cells derived from PBMCs were electroporated on day 3 post-activation using the 4D-Nucleofector™
151 device (Lonza, Basel, Switzerland) following our established protocol(17). Briefly, all ribonucleoprotein
152 (RNP) complexes were pre-assembled by mixing 75 pmol of the guide RNA (GeneScript, Piscataway, NJ)
153 with 18 pmol of Alt-R® S.p. Cas9 Nuclease V3 or Alt-R® S.p. HiFi Cas9 Nuclease V3 (Integrated DNA
154 Technologies, Inc., Coralville, Iowa) and incubated for 10–12 minutes at room temperature. Each RNP
155 complex targeted to each selected site (**Supplementary Table 2**) was prepared separately and combined
156 only immediately before electroporation. After the electroporation pulse, cells were transferred into 96-
157 well plates containing 180 µL of fresh complete RPMI supplemented with 1,000 U/mL rhIL-2 for optimal
158 cell recovery. After 30 minutes, the electroporated cells were transduced with an adeno-associated virus
159 (AAV) serotype 6 encoding a suitable repair template (**Supplementary Table 7**) at a genome copy number
160 of $5x10^4$ GC/cell to achieve the selected *castling* event. Over the next four days, the rhIL-2 concentration

161 was gradually reduced to 100 U/mL. The edited cells were expanded for a total of 14 days and then frozen
162 in CryoStor® CS10 (STEMCELL Technologies, Cologne, Germany) for further use. For the generation of
163 CD19-specific CAR T cells we used a VSV-G pseudotyped lentiviral vector encoding for a second-generation
164 CD19-specific CAR driven by the phosphoglycerate kinase-1 promotor (PGK) promoter. The CAR expression
165 plasmid was generated via Gibson assembly and included the CD19-specific scFV sequence, followed by a
166 CD8 spacer, the 4-1BB/CD3 zeta stimulatory domain and linked via P2A element to a truncated LNGFR
167 used to enrich for CAR+ cells after transduction. The lentiviral particles were purchased using the VSV-G
168 Lentivirus Large-scale Packaging Service for custom vectors (VectorBuilder Inc., Chicago, Illinois). For
169 transduction, $1x10^6$ $CD3^+$ cells were activated as described above and plated in one well of a 48-well plate
170 in activation medium with 1,000 U/mL rhIL-2. Lentiviral particles were added 24 hours later at 5
171 transducing units (TU)/cell, after incubation with Polybrene (final concentration 5 µg/mL; VectorBuilder
172 Inc., Chicago, Illinois) for 5 minutes at room temperature to enhance transduction efficiency. The plate
173 was then spinoculated at 1,600 RCF for 90 minutes to concentrate the virus onto the cell surface.
174 Transduced cells were maintained in culture for two days prior the genome editing procedure conducted
175 as described above.

176 **Cell surface staining and flow cytometry**

177 Cell surface staining was performed using fluorochrome-conjugated primary antibodies for direct
178 detection by flow cytometry. Between $5x10^4$ and $1x10^5$ cells were resuspended in the appropriate
179 antibody mix following the manufacturers' instructions. The following antibodies were used: anti-human
180 CD271 (LNGFR)-APC (clone ME20.4-1.H4, Miltenyi Biotec, Bergisch Gladbach, Germany), anti-human
181 CD25-PE (clone 4E3, Miltenyi Biotec). anti-human CD279-FITC (clone NAT105, BioLegend, San Diego, CA),
182 anti-human CD62L-BV421 (clone DREG-56, BD Horizon, Franklin Lakes, NJ), anti-human CD45RA-FITC
183 (clone HI100, BioLegend), anti-human CD39-BV711 (clone A1, BioLegend), anti-human CD127 (IL-7Rα)-
184 PE/Cy5 (clone A019D5, BioLegend).

185 **Chronic antigen exposure (CAE) assay**

186 Transduced or control T cells were expanded for 14 days in culture with 100 U/mL rhIL-2, with medium
187 exchange every 2–3 days as needed. On the day of assay initiation, LNGFR$^+$ cells (indicative of CAR+ cells
188 as both proteins were co-expressed from the same lentiviral expression cassette) were enriched using the
189 MACS® Cell Separation System and the CD271 (LNGFR) MicroBead Kit (Miltenyi Biotec, Bergisch Gladbach,
190 Germany). This ensured initiation of the assay with a purified (i.e. >95%) CAR$^+$ population. The CAE
191 consisted of co-culturing CD19-specific CAR T cells with CD19$^+$/GFP$^+$ NALM6 cells at a 1:4 effector-to-target
192 (E:T) ratio. As the co-culture progressed, the number of target cells was adjusted to maintain this ratio.
193 Every two days, cells were counted, stained for LNGFR, and analyzed by flow cytometry to determine the
194 number of CAR$^+$ (effector) and GFP$^+$ (target) cells. Based on these counts, the appropriate number of GFP$^+$
195 NALM6 cells was added to sustain the 1:4 ratio. Effector and target cell counts were recorded throughout
196 the assay to monitor CAR T cell proliferation and infer cytotoxic activity. To this end, the number of CAR
197 T cells were quantified as live LNGFR+ cells and cytotoxic activity was calculated as the percentage of live
198 target cells remaining at each time point, relative to the number of target cells initially seeded. The
199 duration required to induce key T cell exhaustion features varied among donors (typically 10–14 days). For
200 miRNA and mRNA sequencing, CAR T cells were separated from the fluorescent target cells by FACS as
201 GFP$^-$ cells (and cryopreserved on days 6, 10, 12, or 14 of the CAE assay). Day 0 samples were collected
202 immediately before assay initiation. Endpoint analyses were performed at the time point when all samples
203 exhibited decrease of the total CAR T cell population (i.e. days 12-14 of the CAE). These analyses included:
204 surface staining for exhaustion and stemness markers (CD39 and IL-7R, respectively); assessment of
205 cytotoxicity by quantifying via flow cytometry the amount of GFP$^+$ cells remaining after an additional 24-
206 hours co-culture at a 1:4 E:T ratio; measurement of cytokine release (IFN-γ and IL-2) using the BD™
207 Cytometric Bead Array (CBA) Human Soluble Protein Master Buffer Kit (BD Biosciences, Franklin Lakes, NJ),
208 according to the manufacturer's instructions.

209 **Sample preparation for the measurement of genome editing efficiency**

210 To determine genome editing efficiency, the regions surrounding the nuclease target sites were PCR-
211 amplified and subjected to next-generation sequencing analysis. In brief, genomic DNA was extracted from
212 frozen pellets of approximately 500,000 cells using a Nucleospin Tissue Extraction Kit (Macherey-Nagel,
213 Düren, Germany). Long or short PCR amplicons were obtained from 100 ng of genomic DNA using the
214 primers indicated in **Supplementary Table 3**. For nested PCR, the long amplicon PCR product was
215 separated on an agarose gel, and the desired band was purified via gel extraction (Qiagen, Germantown,
216 MD 20874, USA). Approximately 20ng of the purified PCR product was used as the input for the nested
217 PCR using the primers indicated in **Supplementary Table 3**. All PCRs were performed with Q5 HotStart
218 polymerase (New England Biolabs GmbH, Frankfurt am Main, Germany), following the manufacturer's
219 instructions.

220 **Quantification of genome editing efficiency**

221 Genome editing efficiency was evaluated by subjecting the PCR amplicons described above to either small
222 or long amplicon sequencing. The small amplicons were used to determine the frequency of indel
223 mutations at the miR-15/16 clusters target sites as well as the precise integration of a small insert (i.e. the
224 mir92b sequence) at the miR-15a/16-1 target on chromosome 13. To this end, small amplicons (500ng of
225 purified PCR product) were sequenced using Illumina paired-end sequencing at Genewiz (Leipzig,
226 Germany) and data analyzed using Crispresso2 (v2.0.20b) with default settings. To quantify the extent of
227 large deletions at the miR-15a/16-1 locus on chromosome 13 and the integration of the large miR-17~92
228 cluster cassette, long read amplicon sequencing was performed using Oxford Nanopore Technology
229 (Microsynth AG, Balgach, Switzerland). The raw reads were filtered using filtlong (version 0.2.1)
230 (min_length 4500) to remove short reads. We then created a BLAST database using the reads of the sample
231 with the “makeblast nucl” command. A series of 6 landmark sequences (the 2 PCR primers, 2gRNAs, the
232 entire inserted sequence and the entire wild-type sequence; **Supplementary Table 8**) were aligned to the

233 sample's database using BLAST (version 2.16.0) using the following parameters: word_size=5, evalue=1,
234 perc_identity=90, dust=no, gapopen=2, gapextend=10, num_alignements=10000000. We parsed the
235 BLAST results of each read and determined the presence of a landmark sequence on the read if the read
236 was successfully aligned to that landmark sequence. In that manner, we evaluated the presence or
237 absence of each landmark sequence in each of the reads. To select complete amplicons, we filtered out all
238 reads that did not have both PCR primer sequences. We lastly sought out to classify reads into 4 groups.
239 The reads containing the wild-type sequence, both gRNA target sequences but not the insertion were
240 classified as "unmodified" reads. The reads missing the gRNA target sequences but containing the inserted
241 sequence were classified as "edited" or "HDR" to indicate that presumably these alleles result from the
242 activation of the HDR-repair pathway leading to precise knock-in events. The reads missing the insertion
243 sequence and at least 1 gRNA target sequence were classified as "cut" or "NHEJ" to indicate that
244 presumably these alleles result from the activation of the NHEJ-repair pathway leading to the formation
245 of variable indel mutations. Lastly, the remaining reads were classified as "other".

246 **Total RNA extraction**

247 Total RNA was extracted from frozen cell pellets containing 10,000–50,000 cells using the miRNeasy Mini
248 Kit (Qiagen, Germany) according to the manufacturer's instructions. Cells were lysed in 1,000 µl QIAzol
249 reagent by mixing on a vortex for 10 seconds. Phase separation was achieved by adding 200 µl chloroform,
250 followed by centrifugation. RNA was precipitated with ethanol in the presence of 50 µg/ml glycogen to
251 enhance the RNA yield. Washing steps were performed automatically on a QIAcube instrument (Qiagen,
252 Germany). RNA was eluted in 30 µl nuclease-free water. RNA concentration and integrity were assessed
253 by spectrophotometry (NanoDrop, absorbance at 260 nm) and microcapillary electrophoresis using the
254 High Sensitivity RNA Kit together with the Fragment Analyzer (Agilent, United States). Purified total RNA
255 samples were stored at –80 °C until further processing.

256 **Measurement of small RNA expression levels**

257 The expression levels of mature miRNA shown in **Supplementary Figure 3c-e** were measured using the
258 TaqMan™ Small RNA Assays" (Applied Biosystems) followed by real time quantitative PCR using TaqMan®
259 Fast Advanced Master Mix (Applied biosystems). In brief, total miRNA was isolated from cells using the
260 miRNeasy Mini Kit (Qiagen) according to the manufacturer's instructions. The selected miRNAs were
261 reverse transcribed using TaqMan™ MicroRNA Reverse Transcription Kit (Applied Biosystems) and
262 quantified using the specific assay IDs: 000389 (hsa-miR-15a-5p), 000391, (has-miR-16-5p), 000390 (hsa-
263 miR-15b-5p) and 002277 (hsa-miR-320a). To obtain relative expression levels, normalization against the
264 reference miRNA 320a was chosen using the 2^-ΔΔCt method(22). For next generation small RNA
265 sequencing, miRNA libraries were prepared from 100 ng total RNA using the RealSeq® Small RNA Library
266 Preparation Kit (RealSeq Biosciences) as previously described(23). Adapter-ligated and reverse-
267 transcribed libraries were quantified by qPCR to determine the optimal number of PCR amplification cycles
268 (17–19 cycles). Amplification was performed using barcoded Illumina reverse primers in combination with
269 the Illumina forward primer. Library quality was assessed using either the DNA 1000 Chip or DNA Fragment
270 Analyzer reagents (Agilent, USA). Equimolar pooling of individually barcoded libraries was performed prior
271 to sequencing on an Illumina NextSeq 2000 instrument with 100 bp single-end reads. Sequencing data
272 were processed using the miND analysis pipeline previously reported(24). Briefly, reads were
273 demultiplexed, and quality was assessed using FastQC and MultiQC. Adapter trimming and quality filtering
274 were performed with Cutadapt, retaining reads ≥17 nt in length. Reads were mapped to the human
275 genome (GRCh38.p14, Ensembl) using Bowtie v1.2.2 allowing up to two mismatches, followed by mapping
276 to miRBase v22.1 (https://www.mirbase.org/) allowing one mismatch, via miRDeep2 v2.0.1.2. Statistical
277 analyses were performed in R v3.6 using the packages pheatmap v1.0.12, pcaMethods v1.78, and
278 genefilter v1.68. Differential expression analysis was conducted with edgeR v3.28, employing quasi-
279 likelihood negative binomial generalized log-linear models. To enhance false discovery rate (FDR) control,
280 the independent filtering approach of DESeq2 was adapted for edgeR to remove low-abundance miRNAs
281 prior to testing.

282 **mRNA sequencing**

283 mRNA-seq libraries were prepared from 100 ng of total RNA using the QuantSeq 3' mRNA-Seq Library Prep
284 Kit FWD for Illumina (Lexogen, Austria) according to the manufacturer's instructions. After library
285 purification, yields were quantified using the Fragment Analyzer (NGS Fragment Kit, Agilent Technologies).
286 Individually barcoded libraries were pooled at equimolar concentrations and sequenced on an Illumina
287 NextSeq 2000 instrument with 100 bp single-end reads. Sequencing data quality was evaluated using
288 FastQC and MultiQC. Adapter trimming and quality filtering were performed using the BBDuk tool (part of
289 the BBMap package, v38.69), retaining reads with a minimum length of 17 nt and Phred quality ≥30. Reads
290 were aligned to the human reference genome (GRCh38.p14, Ensembl) using STAR v2.7, and indexed with
291 SAMtools v1.9. Gene-level read counts were obtained using HTSeq-count v0.13.

292 **Visualization of microRNA and mRNA expression analysis**

293 Heatmaps and principal component analysis (PCA) plots were produced on the basis of ln-transformed
294 RPM data using clustvis(25). For heatmaps unit variance scaling was applied to RPM values and average
295 linkage together with Pearson correlation clustering were used as distance measures. MA plots were
296 produced in Microsoft Excel using log2 fold changes and logCPM values derived from EdgeR differential
297 expression analysis. Volcano plots were generated in R (version ≥4.2) using the *ggplot2* package.
298 Differential expression results were visualized by plotting log2 fold change against −log10 false discovery
299 rate (FDR). Genes were classified as significantly up-regulated or down-regulated using thresholds of FDR
300 < 0.05 and were colored accordingly.

301 **microRNA target prediction and Gene Ontology (GO) enrichment analysis**

302 Target genes for differentially expressed microRNAs were identified using multimiR v1.30.0(26). This tool
303 integrates eight miRNA target prediction databases: DIANA(27), ElMMo(28), MicroCosm(29), PITA(30),
304 miRanda(31), PicTar(32), TargetScan(33) and miRDB(34), as well as three databases with experimentally

305 validated targets: miRTarBase(35), miRecords(36) and TarBase(37). Only target genes found in at least
306 three of the 11 databases were retained for downstream analysis.

307 To identify potential functional miRNA-mRNA interactions, the miRNA results were integrated with
308 differential expression data from mRNA sequencing. The analysis focused exclusively on inverse regulatory
309 relationships, pairing upregulated miRNAs with downregulated mRNAs and downregulated miRNAs with
310 upregulated mRNAs. Differentially expressed mRNAs (FDR ≤ 0.05) between the castled and mock
311 transfected cells at day 0, day 6 or day 10 were used in a GO-term enrichment analysis. Enriched biological
312 processes (BP) were identified by using the Kolmogorov Smirnov (KS) test with the unadjusted p-values
313 from the differential expression analysis as rank information with the tool topGO(38). Gene Ontology (GO)
314 enrichment results were visualized using dot plots generated in R (version ≥4.2) with the ggplot2 package.
315 For each analysis timepoint, the ten most significantly enriched biological process GO terms were selected
316 based on their enrichment score, defined as the negative logarithm (base 10) of the Kolmogorov–Smirnov
317 (KS) test p-value. Dot plots display GO terms on the y-axis and enrichment scores on the x-axis. Dot size
318 corresponds to the number of annotated genes associated with each GO term, while dot color represents
319 the enrichment score using a continuous red-to-blue gradient. GO terms were ordered within each
320 timepoint from highest to lowest enrichment score and displayed side-by-side to enable comparison
321 across timepoints.

322

323 **Results**

324 **Identification of miRNA pairs for *castling***

325 To demonstrate that *castling* can rewire pathological gene networks, we first sought to identify suitable
326 miRNA candidates for swapping. We modified an existing chronic antigen stimulation assay that induces
327 progressive CAR T cell dysfunction, mimicking continuous antigen exposure (**Figure 1b**)(16, 17, 39). To this

328 end, CD19-directed CAR T cells were co-cultured with $CD19^+/GFP^+$ NALM6 leukemia cells for up to 14 days,
329 with tumor cells replenished every two days. Despite donor-to-donor variability, monitoring CAR T cell
330 expansion revealed a reproducible kinetic profile in which proliferation peaked between days 6 and 10,
331 followed by proliferative decline and complete proliferative arrest by day 12-14 (**Supplementary Fig. 1a**).
332 At that point, chronically stimulated CAR T cells displayed additional hallmark features of dysfunction,
333 including declined cytotoxicity and cytokine (IFN-γ and IL-2) production compared to control CAR T cells
334 that were cultured in parallel without antigen exposure (**Supplementary Fig. 1b-d**)(16). Flow cytometric
335 analysis confirmed the acquisition of a dysfunctional phenotype, marked by increased CD39 expression
336 and concomitant loss of the T cell memory marker IL7R in the course of the CAR T and NALM6 cell co-
337 culture (**Supplementary Fig. 1e-f**)(16).

338 We next leveraged this system to capture the temporal dynamics of miRNA expression across the
339 progressive loss of CAR T cell functionality by miRNA sequencing. The analysis was performed at four key
340 time points: day 0 (pre-stimulation), day 6 (a peak of CAR T cell activity), day 10 (a transition phase between
341 function and dysfunction), and day 12/14 (a fully dysfunctional state; **Figure 1b**). The observed dynamics
342 in miRNAs expression were visualized as a heatmap revealing four principal expression profiles (**Figure 1c**):
343 miRNAs progressively upregulated (A) or downregulated (B) in response to antigen stimulation, and
344 miRNAs either peaking at day 6 after initiation of antigen stimulation with expression returning to day 0
345 baseline by days 10-12 (C) or reaching their lowest expression at day 6 of antigen stimulation with rebound
346 to day 0 baseline by day 10 (D). Since day 6 coincided with optimal CAR T cell proliferative capacity
347 (**Supplementary Fig. 1a**), indicative of their functional activation and potency(40), we reasoned that the
348 miRNAs upregulated at this stage (profile C) likely supported their effector function, while those transiently
349 downregulated at this time point (profile D) and upregulated thereafter might promote dysfunction. We
350 therefore suggested that preserving the profile C signature at later time points of antigen exposure
351 concomitantly with inhibiting the profile D signature might preserve CAR T cell functionality during the

352 later phase of chronic antigen stimulation. Accordingly, miRNAs from profile C were selected for swapping
353 into the locus of profile D miRNAs via the *castling* procedure.

354 Among the top candidates from both groups, we selected those displaying the highest fold change of
355 expression on day 6 relative to the pre-stimulation time-point. Notably, most of the top hits from both
356 profiles were miRNA clusters (**Supplementary Table 1**), consistent with their role in coordinating key T cell
357 pathways, as observed in other biological systems(41, 42). As candidates for *castling*, we selected miR-
358 92b-3p together with the miR-17~92 cluster from profile C, and the miR-15/16 clusters from profile D
359 (**Figure 1c, Supplementary Fig. 2, Table 1**). Supporting the biological relevance of these choices, literature
360 evidence indicated that miR-92b-3p and the whole miR-17~92 cluster (profile C) are associated with
361 enhanced lymphocyte activation, expansion and persistence(43, 44) whereas the miR-15/16 clusters
362 (profile D) act to constrain T cell proliferation and survival through regulation of apoptotic and cell-cycle
363 genes(45).

364

365 **Development of TRIPLE: a robust genome editing strategy enabling miRNA *castling***

366 *Castling* requires coordinated knock-out (KO) of the dysfunction-associated miRNA (i.e., from profile D)
367 and simultaneous knock-in (KI), within the same locus, of a protective miRNA counterpart (i.e., from profile
368 C). To achieve this with high efficiency and precision, we developed a novel method to maximize the
369 efficiency of homology-directed repair (HDR) and to allow *castling* to occur in a single, high-fidelity editing
370 step.

371 We first optimized the KO step for the inactivation of the selected detrimental miR-15/16 cluster, present
372 as two copies in the human genome (miR-15a/16-1 on chromosome 13 and miR-15b/16-2 on chromosome
373 3). We tested multiple targeting designs, prioritizing an approach that employed two flanking CRISPR-Cas9
374 complexes to remove the entire cluster regions from both genomic loci simultaneously (**Supplementary**

375 **Fig. 3a-b; Supplementary Table 2**). For the chromosome 3 cluster, we found that deleting miR-16-2 alone
376 (using gRNAs g8 and g9, **Supplementary Fig. 3b**) was sufficient to abolish expression of both miR-16-2 and
377 miR-15b (**Supplementary Fig. 3c-e**), consistent with previously published observations.

378 We next optimized the conditions for the KI step of *castling*. We chose miR-92b as the initial KI candidate,
379 reasoning that its shorter sequence, relative to the miR-17~92 cluster, offered a more practical scenario
380 for evaluating the genome-editing strategy. Transcriptomic analysis indicated that among the two miR-
381 15/16 clusters, the one on chromosome 13 was the most transcriptionally active (**Supplementary Fig. 2**).
382 Therefore, we targeted only this site for insertion of the beneficial miR-92b, while simultaneously
383 inactivating the miR-15b/16-2 cluster on chromosome 3.

384 Using our established T cell genome editing workflow(17, 46), all CRISPR-Cas9 ribonucleoprotein (RNP)
385 complexes were electroporated simultaneously three days after initiation of primary T cell activation,
386 followed by transduction with an AAV6 repair template 30 minutes later (**Figure 2a**). In the absence of the
387 AAV repair template, high editing efficiency at the target locus was observed with ~97% of alleles
388 harboring indel mutations as measured via small amplicon sequencing (**Supplementary Fig. 4a**). To
389 measure the efficiency of precise HDR-mediated insertion, we used an optimized two-step amplification
390 protocol to overcome the challenges posed by long homology arms that exceed the typical 500 bp limit of
391 short-read next generation sequencing (NGS). To this end, a primary PCR using primers external to the
392 homology arms was followed by a nested PCR generating a short, next generation sequencing-compatible
393 amplicon spanning the editing junction (**Supplementary Table 3**). Using this method, we observed only a
394 modest integration efficiency of miR-92b (~7%; **Figure 2c, left panel**), prompting development of a novel
395 approach designed to promote HDR-mediated DNA repair. Since after the initial two-RNP excision, we
396 observed the formation of a predominant deletion at the target locus (**Figure 2b** and **Supplementary Fig.
397 4b**), we hypothesized that adding a third RNP directed to this predominantly deleted region would
398 recurrently generate a double-stranded break, thereby keeping the locus accessible for a longer time and

399 thus promoting HDR-mediated integration of the desired miRNA. We named this approach TRIPLE (for
400 Targeted Replacement Induced by Persistent Locus Editing; **Figure 2b**). Application of TRIPLE led to a
401 striking increase in the insertion efficiency, achieving up to ~70% precise integration of miR-92b at the
402 miR-15a/16-1 locus on chromosome 13, while preserving efficient simultaneous inactivation of the second
403 miR-15/16 cluster on chromosome 3 (**Figure 2c, right panel**). This insertion rate represented an
404 approximately 10-fold improvement over the canonical procedure and effectively eliminated the reads
405 corresponding to the predominant deletion at the target locus on chromosome 13 (**Supplementary Fig.**
406 **4c**). We next attempted *castling* of the larger miR-17~92 cluster, which encodes six miRNAs
407 (**Supplementary Table 1**) within the same locus. While knockout of both miR-15/16 clusters remained
408 highly efficient using the canonical procedure, integration efficiency of the miR-17~92 cluster was initially
409 below detection limit. TRIPLE, however, increased the knock-in efficiency to ~16%, measured via long read
410 amplicon sequencing, demonstrating the scalability of the method also for complex multi-miRNA
411 replacements (**Figure 2c, right panel** and **Supplementary Figure 4d**).

412

413 **Evaluation of coordinate miRNA and mRNA expression profiles in the *castled* T cells**

414 To demonstrate that miRNA *castling* can effectively reprogram gene expression networks, resulting in the
415 anticipated coordinated changes in expression levels of the edited miRNAs and their corresponding target
416 mRNAs, we subjected the *castled* primary T cells described above to a combined bulk miRNA and mRNA
417 sequence analysis. The analysis was performed at the time point typically used as day 0 (pre-antigen
418 stimulation) in our *in vitro* CAR T chronic antigen stimulation assay (**Figure 1b**). Notably, at this pre-
419 stimulation phase, miRNAs of profile D (e.g., miR-15/16 clusters) are already expressed at higher level as
420 compared to the majority of those belonging to profile C (**Figure 1c** and **Supplementary Figure 2**).

421 We next focused on the analysis of expression levels of the specific miRNAs used for *castling*. In line with
422 the expectations, edited T cells displayed strong downregulation of all miR-15/16 cluster members and a
423 corresponding increase in expression of the inserted miRNAs, with miR-92b reaching a 4.4-fold increase,
424 while the individual members of the miR-17~92 cluster were upregulated between 1.6-fold and 2.6-fold
425 relative to mock controls (**Supplementary Fig. 5, left panel**), consistent with the higher insertion efficiency
426 of the single miRNA compared to the miRNA cluster (70.8% vs 16.1%, respectively; **Figure 2c)**. Importantly,
427 all miRNA isoforms (isomiRs) derived from the targeted clusters followed the same regulatory direction,
428 demonstrating precise modulation across both canonical and variant sequences (**Supplementary Fig. 5,**
429 **right panel**).

430 To determine whether these changes were accompanied by coordinated mRNA responses, we analyzed
431 global mRNA expression in the same samples in the cells where miR-17~92 cluster was inserted into the
432 miR-15a/16-1 locus on chromosome 13, as this configuration was expected to elicit broader downstream
433 effects than castling of the single miR-92b. Among more than 500 statistically significant (FDR < 0.05)
434 expressed genes identified in the *castled* samples as compared to the mock control sample, approximately
435 half of them were predicted targets of the *castled* miRNAs. Of these, ~75% exhibited inverse regulation
436 relative to their corresponding miRNA partners, consistent with canonical miRNA-mediated mRNA
437 repression (**Figure 2f**). The lists of genes identified as inversely regulated compared to either miR-15/16 or
438 miR-17~92 cluster members are displayed in **Supplementary Tables 4** and **5,** respectively. These findings
439 confirm that *castling* of selected miRNA sequences rewires downstream gene expression, largely in the
440 expected direction. Next, we investigated whether molecular changes elicited by *castling* in primary T cells
441 translate into measurable functional benefits when applied to engineered CAR T cells exposed to chronic
442 antigen stimulation.

443

444 ***Castling* of miR-17~92 and miR-15a/16-1 elicits mRNA expression profile supporting CAR T effector**
445 **function and delays the onset of CAR T cell dysfunction under chronic antigen stimulation**

446 As indicated above, the functional impact of *castling*-mediated gene networks rewiring in CAR T cells was
447 assessed by focusing on insertion of the miR-17~92 cluster into the miR-15a/16-1 locus on chromosome
448 13, with simultaneous inactivation of the second miR-15/16 cluster on chromosomes 3. We hypothesized
449 that *castling* would sustain CAR T cell effector function during chronic antigen stimulation by maintaining
450 high miR-17~92 expression through its integration at the miR-15a/16-1 locus, while simultaneously
451 suppressing the dysfunction-promoting miR-15/16 program via genomic knockout.

452 The experimental design followed the outline shown in **Figure 1b** with *castling* performed using the
453 established TRIPLE-based workflow two days after the CAR cassette transduction. Edited and control cells
454 were expanded for 12 days prior to initiation of chronic antigen stimulation and were harvested for
455 analysis before antigen exposure (day 0) and after 6 and 10 of stimulation. Genome editing efficiency was
456 assessed via long-read sequencing prior to initiation of the chronic antigen stimulation, revealing that
457 approximately 50% of reads showed evidence of indel mutations as a result of nuclease activity, indicative
458 of efficient inactivation of the targeted miR-15a/16-1 locus. Additionally, ~15% of the reads corresponded
459 to precise knock-in events of the miR-17~92 cluster at the chromosome 13 target site**,** consistent with
460 previous results in primary T cells (**Figure 3a**).

461 To track miRNA expression dynamics, miRNA sequencing was performed at days 0, 6, and 10. Consistent
462 with the *castling* strategy, edited CAR T cells displayed an efficient ablation of the endogenous miR-15/16
463 clusters expression, accompanied by a sustained upregulation of all miR-17~92 cluster members (**Figure**
464 **3b**). Unlike their physiological transient expression in mock controls, which peaked at day 6 and declined
465 thereafter, in the edited cells, the expression of miR-17~92 cluster members remained persistently
466 elevated while miR-15/16 clusters expression was suppressed throughout the assay (**Supplementary Fig.**

467 **6**), supporting the underlying hypothesis that *castling*-mediated rewiring of promoter control can maintain
468 beneficial regulatory programs over time.

469 Functionally, these molecular changes translated into measurable performance gains of the *castled* CAR T
470 cells. During repeated antigen exposure, *castled* CAR T cells maintained >90% tumor cell killing ability up
471 to day 8 of antigen stimulation, as measured by counting the remaining NALM6 cells at the specific time
472 points before replenishing them, while control CAR T cells showed an early functional decline, with
473 cytotoxicity falling to ~75% by that time (**Supplementary Fig. 7a**). In line with their enhanced cytolytic
474 potential, flow cytometric analysis at the assay end point revealed a modest but consistent increase in the
475 frequency of $CD8^+$ effector T cells in the *castled* sample (**Supplementary Fig. 7b**).

476 To assess the impact of *castling* on CAR T cell gene expression, we performed bulk mRNA sequencing and
477 visualized differentially expressed genes in volcano plots comparing *castled* cells to their respective mock
478 control counterparts at each time point (**Figure 3c, upper panel**). Consistent with progressive cellular
479 remodeling induced by persistent antigen stimulation, the number of significantly differentially expressed
480 genes (FDR <0.05) increased over time, reflecting the dynamic reshaping of the transcriptional landscape
481 as the assay progressed. This observation was also confirmed by the principal component analysis (PCA)
482 demonstrating substantial gene expression differences between the two cell subsets on day 10
483 (**Supplementary Fig. 8**).

484 Gene Ontology (GO) analysis provided functional insight into these transcriptional changes (**Figure 3c,**
485 **lower panel**). At day 0, the primary differences between *castled* and control cells were observed in
486 metabolic and biosynthetic processes. By the intermediate day 6 time point, enriched GO terms
487 predominantly reflected responses to antigenic stimuli, including viral, biotic, and other organisms (**Figure**
488 **3c, lower panel**) suggesting that *castled* cells were more reactive relative to controls. At the endpoint (day
489 10), numerous GO terms related to T cell activation were strongly enriched, in agreement with the

490 increased proportion of CD8$^+$ cells at this time point (**Supplementary Fig. 7b**) and consistent with the
491 rewired cells adopting a more terminally differentiated cytotoxic phenotype.

492 At this latter time point, about 500 genes were significantly deregulated (FDR <0.05) with expression
493 changes of at least 2-fold (**Supplementary Table 6**). Several genes known to enhance CAR T cell effector
494 function were upregulated, including those associated with increased invasiveness (*CCL5* – ~5-fold
495 upregulation)(47), improved antigen recognition (*KLRC4*, *AOAH* – ~3-4-fold upregulation)(48, 49),
496 enhanced cytotoxicity (*CD8A/B*, *ITGAE*, *SYTL2*, *GNLY*, *NKG7*, *SLAMF7, IL2RB* – ~2-4-fold upregulation)(50-
497 56), improved survival and persistence (*KIT, CD27, SLAMF6* - ~2-9-fold upregulation)(57-59), enhanced
498 proliferation and heightened activation (*JAML, CRACR2A, CD63* – ~2-3 fold upregulation)(60-62). Whereas
499 upregulation of CD8A/B could be a reflection of a higher proportion of CD8+ cells among the *castled* ones
500 (**Supplementary Fig. 7b**), the detected 4-fold and 7-fold significant upregulation of *TRGC1* and *TRGC2*,
501 respectively, in the *castled* cells could be a reflection of a higher proportion of γδ T-cell lineage known for
502 their contribution to rapid cytotoxicity, cytokine secretion and tissue surveillance(63). Conversely, a
503 notable set of genes linked to Type I interferon (IFN) response (*IFI44L*, *IFI44*, *IFIT3*, *MX2*, *RSAD2* and *OAS2*),
504 known for hampering CAR T cell antitumor function(64, 65), were downregulated up to 20-fold.
505 Additionally, expression of most of the IFN response genes mentioned above has been individually
506 confirmed as detrimental for CAR T effector function(66-69). Among other known genes whose damped
507 expression has been previously associated with improved T cell effector function and persistence,
508 *SOX4(16)*, *LGALS1(70), SOCS1(71), LGALS9(72), ARG2(73), PTGS2(74), SESN3(75),* and *CD38(76)* were found
509 downregulated up to 8-fold.

510 Together, these results provide proof-of-concept that *castling* of rationally selected miRNAs can
511 functionally reprogram CAR T cells, sustaining effector capacity under chronic antigen stimulation.

512

513 **Discussion**

514 Our results demonstrate that *castling* can rewire complex pathology-driven gene regulatory networks to
515 sustain effector function of engineered CAR T cells under chronic antigen stimulation compared to non-
516 modified CAR T cells. This entails the coordinated upregulation of numerous beneficial genes and
517 downregulation of detrimental ones, in line with several literature reports correlating the expression of
518 these genes with enhancement of specific aspects of CAR T or T cell function. By orchestrating these
519 changes simultaneously, this approach achieves a holistic reprogramming that extends beyond
520 conventional strategies for CAR T cells enhancement.

521 *Castling* involves a single genome editing step, in which miRNA sequence(s) that counteract the disease
522 state and are insufficiently expressed under pathological conditions are inserted into the genomic locus of
523 a disease-promoting miRNA. Because this locus is transcriptionally activated in the disease state, *castling*
524 simultaneously suppresses the pathogenic program while inducing a beneficial one (**Figure 1a**). Hence, the
525 potential therapeutic gain of *castling* is two-fold: (1) activation of the "therapeutic program" through a
526 disease-triggered promoter, thus ensuring its execution under pathological conditions of interest via using
527 the disease's own transcriptional machinery against itself; and (2) inhibition of the "disease program" that
528 is usually triggered by pathology from the unmodified locus into which insertion has been performed.
529 Although not addressed in this study, a third advantage - an automatic winding down of the *castled*
530 therapeutic program once the pathological trigger has gone - can be theoretically anticipated.

531 To enable efficient *castling* at the genomic level, we developed TRIPLE (Targeted Replacement Induced by
532 Persistent Locus Editing). This novel genome editing procedure uses two RNPs to generate a defined
533 excision at the target locus, creating a predominant and predictable deletion allele. A third RNP is then
534 directed to this newly formed junction, enabling recurrent cleavage of the edited chromosome. Although
535 the precise mechanism remains to be fully elucidated, this repeated targeting likely prolongs the window
536 during which the locus remains accessible to homology-directed repair, thereby markedly improving

537 knock-in efficiency. Importantly, the conceptual simplicity of TRIPLE, unlike previous double-tap or
538 recursive editing strategies relying on microhomology(77, 78), suggests that it should be broadly applicable
539 to diverse genomic contexts. Importantly, other emerging genome engineering technologies could, in
540 principle, also be adapted to achieve targeted sequence insertion. These include e.g. prime editing(79),
541 CRISPR-associated transposases (CAST)(80), recombinase- or integrase-based systems such as PASTE(81),
542 and homology-independent targeted integration (HITI)(82). Each of these platforms offers distinct
543 advantages with respect to cargo size, repair pathway usage, or genomic flexibility. However, they mostly
544 require specialized molecular components, complex optimization, or non-canonical enzymes that may
545 limit immediate applicability across diverse loci and cell types as well accessibility for a broad community
546 of researchers. In contrast, TRIPLE builds on well-established CRISPR–Cas9 editing workflows and achieves
547 substantial gains in knock-in efficiency through the simple addition of an extra guide RNA, making it
548 straightforward to implement, broadly accessible, and readily compatible with existing *ex vivo* cell
549 engineering pipelines.

550 Our data confirmed that *castling* could efficiently place the selected "therapeutic" miRNAs (miR-92b or
551 the members of the miR-17~92 cluster) under the regulatory elements of the target "pathogenic" miRNA
552 (miR-15a/16-1) while disrupting the expression of the latter with concomitant inverse regulation of
553 numerous mRNAs predicted to be targeted by the *castled* miRNAs. Importantly, *castling*-dependent
554 rewiring can sustain beneficial regulatory programs over time, and, unlike their transient physiological
555 expression in non-edited cells, the *castled* miR-17~92 cluster members remained elevated in modified CAR
556 T cells throughout chronic antigen stimulation. In our experiment, being performed in unstimulated T cells,
557 *castling* also likely "primed" CAR T cells obtained from this cell population, so that upon the onset of
558 chronic antigen-stimulation elicited dysfunction, the protective miRNAs could be rapidly and robustly
559 upregulated from the disease(pathology)-activated promoter to levels far above normal, positioning the
560 cells to sustain beneficial gene expression programs when they are mostly needed.

561 Notably, the model of CAR T cell dysfunction used in our study mimics a well-known phenomenon of CAR
562 T cell exhaustion, the phenotype that they typically acquire upon entering the tumor microenvironment
563 as shown in multiple instances and that limits their therapeutic potential(16-18). However, we emphasize
564 that the *castled* CAR T cells presented here are not yet optimized for clinical use; the primary aim of these
565 experiments was to provide a technical proof of concept for the feasibility of this novel methodology. The
566 cells have not yet been tested *in vivo,* which will be addressed in future studies. Furthermore, although
567 the observed gene expression changes and functional assays support enhanced effector function of the
568 *castled* cells, the optimal miRNA pairs or clusters for *castling* may remain to be identified. In addition, the
569 efficiency and specificity of *castling* may be further improved beyond what was achieved in the present
570 study, for example through optimization of repair templates(83) or the use of genome-editing systems
571 with enhanced homology-directed repair activity(84).

572 In conclusion, *castlin*g provides a versatile framework for miRNA-guided network reprogramming, with
573 TRIPLE enabling high-efficiency, precise genome editing not only for single miRNAs but also for miRNA
574 clusters. By harnessing endogenous regulatory logic to modulate gene networks, *castling* enables single-
575 event, multi-target tuning of cellular programs, offering a versatile blueprint for engineering resilient cell
576 therapies. Beyond potential implications in improving CAR T cell therapy, miRNA *castling* may also be used
577 *ex vivo* for improvement of other therapeutically relevant cell types, including macrophages, NK cells,
578 Tregs and various types of stem cells. With appropriate delivery systems, this approach holds a
579 transformative potential also for *in vivo* interventions against complex chronic diseases, such as
580 neurodegeneration, cardiovascular disorders, autoimmune diseases and fibrosis, driven by complex
581 regulatory gene expression imbalances. Finally, *castling* may be applicable not only for swapping
582 “pathogenic” and “therapeutic” miRNAs but also of “pathogenic” and “therapeutic” protein coding mRNAs
583 either between them or with miRNA if and when it deems therapeutically appropriate.

584

585 **Conclusion**

586 In summary, our study demonstrates that *castling* can efficiently rewire disease-associated gene
587 regulatory networks in a single genome-editing step, sustaining beneficial miRNA programs while
588 suppressing pathogenic ones. Implemented via the TRIPLE methodology, this approach achieves high-
589 efficiency, precise editing of both individual miRNAs and miRNA clusters, enabling durable modulation of
590 cellular programs under chronic stress conditions. Beyond providing a proof-of-concept for improving CAR
591 T cell function, *castling* represents a versatile framework for *in vitro* or potentially *in vivo* reprogramming
592 of therapeutically relevant cells. By harnessing endogenous regulatory mechanisms, this strategy offers a
593 broadly applicable blueprint for correcting complex regulatory imbalances in diverse diseases, from
594 immune dysfunction and cancer to chronic inflammatory and degenerative disorders, highlighting its
595 transformative potential for next-generation cell and gene therapies.

596

597 **Declarations**

598 Ethics approval and consent to participate: not applicable

599 Consent for publication: not applicable

600 Availability of data and materials: The sequencing data generated in this study are deposited in the gene
601 expression omnibus (GEO) database with the accession number GSE316480.

602 Competing interests: H.K., S.A., S.A.N., E.S., D.Z. are employed at Lepton Pharmaceuticals. M.H., M.P. and
603 A.D. are employed at TAmiRNA GmbH. E.F. and C.M. are advisors to Lepton Pharmaceuticals. T.C. is an
604 advisor to AaviGen, AstraZeneca, Cimeio Therapeutics, Excision BioTherapeutics, GenCC, and Novo
605 Nordisk. All other authors declare no conflicts of interest.

606 Funding: This study was supported by Lepton Pharmaceuticals and institutional funds to C.M. We also
607 acknowledge funding from the UK National Centre for the Replacement, Refinement and Reduction of
608 Animals in Research (NC3Rs) CRACK IT Challenge NC/C022201/01 (T.C., M.S.R.A., M.B., A.T.), and the
609 German Federal Ministry of Research, Technology and Space (BMFTR) within the Medical Informatics
610 Funding Scheme PM4Onco–FKZ 01ZZ2322A (M.B.), EkoEstMed–FKZ 01ZZ2015 (G.A.). The article
611 processing charge was funded by the University of Freiburg's Open Access Publishing funding program.

612 Authors' contributions: E.F and C.M. conceived the ideas of castling and TRIPLE, respectively. D.A, M.S.R.A,
613 H.K., S.A, S.A.N., E.S., D.Z. and C.M. designed the study. D.A, M.S.R.A, M.P., M.R., A.T. and A.D. performed
614 experiments. D.A, M.S.R.A, H.K., S.A., M.P., A.T., A.D., G.A., M.H., D.Z., E.F. and C.M. analyzed data. M.B.,
615 T.I.C., D.Z., T.C. and C.M. acquired funding. D.Z., E.F. and C.M. wrote the paper with input from all authors.

616 Acknowledgements: We would like to thank all the members of the Institute for Transfusion Medicine and
617 Gene Therapy's R&D department, Juliana Friedman (Lepton Pharmaceuticals), Dr. Elena Sotillo (Senior
618 Research Scientist, Stanford Cancer Institute, Stanford University, Palo Alto, USA) and Dimitrios L. Wagner
619 (Institute of Medical Immunology, Charité – Universitätsmedizin Berlin, Berlin, Germany) for productive
620 discussions. Special thanks to Antonio Carusillo, Jamal Alzubi, Sibtain Haider, Michalis Papacharalampous
621 and Melissa Whitehead for scientific advice. We are grateful to the FREEZE Biobank, the Blood Donation
622 Center, and the Lighthouse Core facility, all Medical Center-University of Freiburg, for provision of the LRS
623 chambers containing the PBMCs of healthy donors, or help with flow cytometry, respectively.

624

625 **References**

626 1. Lee TI, Young RA. Transcriptional regulation and its misregulation in disease. Cell.
627 2013;152(6):1237-51.
628 2. Wang J, Liu Q, Shyr Y. Dysregulated transcription across diverse cancer types reveals the
629 importance of RNA-binding protein in carcinogenesis. BMC genomics. 2015;16 Suppl 7(Suppl 7):S5.

630 3. Hu Z, You L, Hu S, Yu L, Gao Y, Li L, et al. Hepatocellular carcinoma cell-derived exosomal miR-21-
631 5p promotes the polarization of tumor-related macrophages (TAMs) through SP1/XBP1 and affects the
632 progression of hepatocellular carcinoma. Int Immunopharmacol. 2024;126:111149.
633 4. Kim J, Ha S, Son M, Kim D, Kim MJ, Kim B, et al. TLR7 activation by miR-21 promotes renal fibrosis
634 by activating the pro-inflammatory signaling pathway in tubule epithelial cells. Cell Commun Signal.
635 2023;21(1):215.
636 5. Kurowska-Stolarska M, Alivernini S, Ballantine LE, Asquith DL, Millar NL, Gilchrist DS, et al.
637 MicroRNA-155 as a proinflammatory regulator in clinical and experimental arthritis. Proc Natl Acad Sci U
638 S A. 2011;108(27):11193-8.
639 6. Pasculli B, Barbano R, Fontana A, Biagini T, Di Viesti MP, Rendina M, et al. Hsa-miR-155-5p Up-
640 Regulation in Breast Cancer and Its Relevance for Treatment With Poly[ADP-Ribose] Polymerase 1 (PARP-
641 1) Inhibitors. Frontiers in oncology. 2020;10:1415.
642 7. Hsu CH, Liu IF, Kuo HF, Li CY, Lian WS, Chang CY, et al. miR-29a-3p/THBS2 Axis Regulates PAH-
643 Induced Cardiac Fibrosis. International journal of molecular sciences. 2021;22(19).
644 8. Li L, He X, Liu M, Yun L, Cong B. Diagnostic value of cardiac miR-126-5p, miR-134-5p, and miR-
645 499a-5p in coronary artery disease-induced sudden cardiac death. Front Cardiovasc Med.
646 2022;9:944317.
647 9. Beg MS, Brenner AJ, Sachdev J, Borad M, Kang YK, Stoudemire J, et al. Phase I study of MRX34, a
648 liposomal miR-34a mimic, administered twice weekly in patients with advanced solid tumors. Invest New
649 Drugs. 2017;35(2):180-8.
650 10. Diener C, Keller A, Meese E. Emerging concepts of miRNA therapeutics: from cells to clinic.
651 Trends Genet. 2022;38(6):613-26.
652 11. Viteri S, Rosell R. An innovative mesothelioma treatment based on miR-16 mimic loaded EGFR
653 targeted minicells (TargomiRs). Transl Lung Cancer Res. 2018;7(Suppl 1):S1-S4.
654 12. Grimm D, Streetz KL, Jopling CL, Storm TA, Pandey K, Davis CR, et al. Fatality in mice due to
655 oversaturation of cellular microRNA/short hairpin RNA pathways. Nature. 2006;441(7092):537-41.
656 13. Segal M, Slack FJ. Challenges identifying efficacious miRNA therapeutics for cancer. Expert Opin
657 Drug Discov. 2020;15(9):987-92.
658 14. Hong DS, Kang YK, Borad M, Sachdev J, Ejadi S, Lim HY, et al. Phase 1 study of MRX34, a
659 liposomal miR-34a mimic, in patients with advanced solid tumours. British journal of cancer.
660 2020;122(11):1630-7.
661 15. Liu YP, Berkhout B. miRNA cassettes in viral vectors: problems and solutions. Biochim Biophys
662 Acta. 2011;1809(11-12):732-45.
663 16. Good CR, Aznar MA, Kuramitsu S, Samareh P, Agarwal S, Donahue G, et al. An NK-like CAR T cell
664 transition in CAR T cell dysfunction. Cell. 2021;184(25):6081-100 e26.
665 17. Roman Azcona MS, Monaco G, Whitehead M, Kaufmann MM, Alzubi J, Cathomen T, et al.
666 Sustained and specific multiplexed immune checkpoint modulation in CAR T cells induced by targeted
667 epigenome editing. Molecular therapy Nucleic acids. 2025;36(3):102618.
668 18. Locke FL, Filosto S, Chou J, Vardhanabhuti S, Perbost R, Dreger P, et al. Impact of tumor
669 microenvironment on efficacy of anti-CD19 CAR T cell therapy or chemotherapy and transplant in large B
670 cell lymphoma. Nat Med. 2024;30(2):507-18.
671 19. Yan ZX, Li L, Wang W, OuYang BS, Cheng S, Wang L, et al. Clinical Efficacy and Tumor
672 Microenvironment Influence in a Dose-Escalation Study of Anti-CD19 Chimeric Antigen Receptor T Cells
673 in Refractory B-Cell Non-Hodgkin's Lymphoma. Clinical cancer research : an official journal of the
674 American Association for Cancer Research. 2019;25(23):6995-7003.
675 20. Liu X, Zhang Y, Li K, Liu Y, Xu J, Ma J, et al. A novel dominant-negative PD-1 armored anti-CD19
676 CAR T cell is safe and effective against refractory/relapsed B cell lymphoma. Transl Oncol.
677 2021;14(7):101085.

678 21. John LB, Devaud C, Duong CP, Yong CS, Beavis PA, Haynes NM, et al. Anti-PD-1 antibody therapy
679 potently enhances the eradication of established tumors by gene-modified T cells. Clinical cancer
680 research : an official journal of the American Association for Cancer Research. 2013;19(20):5636-46.
681 22. Livak KJ, Schmittgen TD. Analysis of relative gene expression data using real-time quantitative
682 PCR and the 2(-Delta Delta C(T)) Method. Methods. 2001;25(4):402-8.
683 23. Khamina K, Diendorfer AB, Skalicky S, Weigl M, Pultar M, Krammer TL, et al. A MicroRNA Next-
684 Generation-Sequencing Discovery Assay (miND) for Genome-Scale Analysis and Absolute Quantitation of
685 Circulating MicroRNA Biomarkers. International journal of molecular sciences. 2022;23(3).
686 24. Diendorfer A, Khamina K, Pultar M, Hackl M. miND (miRNA NGS Discovery pipeline): a small RNA-
687 seq analysis pipeline and report generator for microRNA biomarker discovery studies. F1000Research.
688 2022;11.
689 25. Metsalu T, Vilo J. ClustVis: a web tool for visualizing clustering of multivariate data using Principal
690 Component Analysis and heatmap. Nucleic Acids Res. 2015;43(W1):W566-70.
691 26. Ru Y, Kechris KJ, Tabakoff B, Hoffman P, Radcliffe RA, Bowler R, et al. The multiMiR R package
692 and database: integration of microRNA-target interactions along with their disease and drug
693 associations. Nucleic Acids Res. 2014;42(17):e133.
694 27. Maragkakis M, Reczko M, Simossis VA, Alexiou P, Papadopoulos GL, Dalamagas T, et al. DIANA-
695 microT web server: elucidating microRNA functions through target prediction. Nucleic Acids Res.
696 2009;37(Web Server issue):W273-6.
697 28. Gaidatzis D, van Nimwegen E, Hausser J, Zavolan M. Inference of miRNA targets using
698 evolutionary conservation and pathway analysis. BMC Bioinformatics. 2007;8:69.
699 29. Griffiths-Jones S, Saini HK, van Dongen S, Enright AJ. miRBase: tools for microRNA genomics.
700 Nucleic Acids Res. 2008;36(Database issue):D154-8.
701 30. Kertesz M, Iovino N, Unnerstall U, Gaul U, Segal E. The role of site accessibility in microRNA
702 target recognition. Nat Genet. 2007;39(10):1278-84.
703 31. Betel D, Wilson M, Gabow A, Marks DS, Sander C. The microRNA.org resource: targets and
704 expression. Nucleic Acids Res. 2008;36(Database issue):D149-53.
705 32. Anders G, Mackowiak SD, Jens M, Maaskola J, Kuntzagk A, Rajewsky N, et al. doRiNA: a database
706 of RNA interactions in post-transcriptional regulation. Nucleic Acids Res. 2012;40(Database issue):D180-
707 6.
708 33. Friedman RC, Farh KK, Burge CB, Bartel DP. Most mammalian mRNAs are conserved targets of
709 microRNAs. Genome Res. 2009;19(1):92-105.
710 34. Wang X. miRDB: a microRNA target prediction and functional annotation database with a wiki
711 interface. Rna. 2008;14(6):1012-7.
712 35. Hsu SD, Lin FM, Wu WY, Liang C, Huang WC, Chan WL, et al. miRTarBase: a database curates
713 experimentally validated microRNA-target interactions. Nucleic Acids Res. 2011;39(Database
714 issue):D163-9.
715 36. Xiao F, Zuo Z, Cai G, Kang S, Gao X, Li T. miRecords: an integrated resource for microRNA-target
716 interactions. Nucleic Acids Res. 2009;37(Database issue):D105-10.
717 37. Vergoulis T, Vlachos IS, Alexiou P, Georgakilas G, Maragkakis M, Reczko M, et al. TarBase 6.0:
718 capturing the exponential growth of miRNA targets with experimental support. Nucleic Acids Res.
719 2012;40(Database issue):D222-9.
720 38. Alexa A, Rahnenfuhrer J. topGO: Enrichment analysis for Gene Ontology. R package version 2.28.
721 0. Cranio. 2016;2:11.
722 39. Dai X, Park JJ, Du Y, Na Z, Lam SZ, Chow RD, et al. Massively parallel knock-in engineering of
723 human T cells. Nat Biotechnol. 2023;41(9):1239-55.
724 40. Shao L, Zheng Y, Somerville RP, Stroncek DF, Jin P. New insights on potency assays from recent
725 advances and discoveries in CAR T-cell therapy. Frontiers in immunology. 2025;16:1597888.

726 41. Guo L, Zhao Y, Zhang H, Yang S, Chen F. Integrated evolutionary analysis of human miRNA gene
727 clusters and families implicates evolutionary relationships. Gene. 2014;534(1):24-32.
728 42. Wang Y, Luo J, Zhang H, Lu J. microRNAs in the Same Clusters Evolve to Coordinately Regulate
729 Functionally Related Genes. Molecular biology and evolution. 2016;33(9):2232-47.
730 43. Jiang S, Li C, Olive V, Lykken E, Feng F, Sevilla J, et al. Molecular dissection of the miR-17-92
731 cluster's critical dual roles in promoting Th1 responses and preventing inducible Treg differentiation.
732 Blood. 2011;118(20):5487-97.
733 44. Li M, Shan W, Hua Y, Chao F, Cui Y, Lv L, et al. Exosomal miR-92b-3p Promotes Chemoresistance
734 of Small Cell Lung Cancer Through the PTEN/AKT Pathway. Front Cell Dev Biol. 2021;9:661602.
735 45. Gagnon JD, Kageyama R, Shehata HM, Fassett MS, Mar DJ, Wigton EJ, et al. miR-15/16 Restrain
736 Memory T Cell Differentiation, Cell Cycle, and Survival. Cell reports. 2019;28(8):2169-81 e4.
737 46. Dibas A, Rhiel M, Patel VB, Andrieux G, Boerries M, Cornu TI, et al. Cell-Based Models of
738 'Cytokine Release Syndrome' Endorse CD40L and Granulocyte-Macrophage Colony-Stimulating Factor
739 Knockout in Chimeric Antigen Receptor T Cells as Mitigation Strategy. Cells. 2023;12(21).
740 47. Tian Y, Zhang L, Ping Y, Zhang Z, Yao C, Shen C, et al. CCR5 and IL-12 co-expression in CAR T cells
741 improves antitumor efficacy by reprogramming tumor microenvironment in solid tumors. Cancer
742 immunology, immunotherapy : CII. 2025;74(2):55.
743 48. Gong L, Luo J, Yang E, Ru B, Qi Z, Yang Y, et al. Cancer immunology data engine reveals secreted
744 AOAH as a potential immunotherapy. Cell. 2025;188(18):5062-80 e32.
745 49. Tan W, Liu M, Wang L, Guo Y, Wei C, Zhang S, et al. Novel immune-related genes in the tumor
746 microenvironment with prognostic value in breast cancer. BMC cancer. 2021;21(1):126.
747 50. Kagoya Y, Tanaka S, Guo T, Anczurowski M, Wang CH, Saso K, et al. A novel chimeric antigen
748 receptor containing a JAK-STAT signaling domain mediates superior antitumor effects. Nat Med.
749 2018;24(3):352-9.
750 51. Laugel B, Cole DK, Clement M, Wooldridge L, Price DA, Sewell AK. The multiple roles of the CD8
751 coreceptor in T cell biology: opportunities for the selective modulation of self-reactive cytotoxic T cells. J
752 Leukoc Biol. 2011;90(6):1089-99.
753 52. Li C, Ligons DL, Lanasa D, Keller HR, Luckey MA, Capaldo B, et al. Integrin CD103 expression in
754 naive CD8(+) T cells promotes cytokine-driven acquisition of memory phenotype and effector function.
755 Immunity. 2025;58(11):2734-52 e9.
756 53. Lingel H, Fischer L, Remstedt S, Kuropka B, Philipsen L, Han I, et al. SLAMF7 (CD319) on activated
757 CD8(+) T cells transduces environmental cues to initiate cytotoxic effector cell responses. Cell Death
758 Differ. 2025;32(3):561-72.
759 54. Menasche G, Menager MM, Lefebvre JM, Deutsch E, Athman R, Lambert N, et al. A newly
760 identified isoform of Slp2a associates with Rab27a in cytotoxic T cells and participates to cytotoxic
761 granule secretion. Blood. 2008;112(13):5052-62.
762 55. Saini RV, Wilson C, Finn MW, Wang T, Krensky AM, Clayberger C. Granulysin delivered by
763 cytotoxic cells damages endoplasmic reticulum and activates caspase-7 in target cells. Journal of
764 immunology. 2011;186(6):3497-504.
765 56. Dong H, Ham H, Barham W, Wen T, Hirdler JB, Mao Z, et al. A Dual Role for NKG7 in T-cell
766 Cytotoxicity and Longevity. Cancer immunology research. 2025;13(10):1510-5.
767 57. Hendriks J, Gravestein LA, Tesselaar K, van Lier RA, Schumacher TN, Borst J. CD27 is required for
768 generation and long-term maintenance of T cell immunity. Nature immunology. 2000;1(5):433-40.
769 58. Oba T, Long MD, Ito KI, Ito F. Clinical and immunological relevance of SLAMF6 expression in the
770 tumor microenvironment of breast cancer and melanoma. Scientific reports. 2024;14(1):2394.
771 59. Xiong Y, Taleb M, Misawa K, Hou Z, Banerjee S, Amador-Molina A, et al. c-Kit signaling
772 potentiates CAR T cell efficacy in solid tumors by CD28- and IL-2-independent co-stimulation. Nat Cancer.
773 2023;4(7):1001-15.

774 60. Hao Z, Xin Z, Chen Y, Shao Z, Lin W, Wu W, et al. JAML promotes the antitumor role of tumor-
775 resident CD8(+) T cells by facilitating their innate-like function in human lung cancer. Cancer letters.
776 2024;590:216839.
777 61. Pfistershammer K, Majdic O, Stockl J, Zlabinger G, Kirchberger S, Steinberger P, et al. CD63 as an
778 activation-linked T cell costimulatory element. Journal of immunology. 2004;173(10):6000-8.
779 62. Woo JS, Srikanth S, Kim KD, Elsaesser H, Lu J, Pellegrini M, et al. CRACR2A-Mediated TCR
780 Signaling Promotes Local Effector Th1 and Th17 Responses. Journal of immunology. 2018;201(4):1174-
781 85.
782 63. Di Simone M, Corsale AM, Toia F, Shekarkar Azgomi M, Di Stefano AB, Lo Presti E, et al. Tumor-
783 infiltrating gammadelta T cells as targets of immune checkpoint blockade in melanoma. J Leukoc Biol.
784 2024;115(4):760-70.
785 64. Jung IY, Bartoszek RL, Rech AJ, Collins SM, Ooi SK, Williams EF, et al. Type I Interferon Signaling
786 via the EGR2 Transcriptional Regulator Potentiates CAR T Cell-Intrinsic Dysfunction. Cancer Discov.
787 2023;13(7):1636-55.
788 65. Sun S, Zhi Z, Su Y, Sun J, Li Q. A CD8(+) T cell-associated immune gene panel for prediction of the
789 prognosis and immunotherapeutic effect of melanoma. Frontiers in immunology. 2022;13:1039565.
790 66. Chen GM, Chen C, Das RK, Gao P, Chen CH, Bandyopadhyay S, et al. Integrative Bulk and Single-
791 Cell Profiling of Premanufacture T-cell Populations Reveals Factors Mediating Long-Term Persistence of
792 CAR T-cell Therapy. Cancer Discov. 2021;11(9):2186-99.
793 67. Dar AA, Pradhan TN, Kulkarni DP, Shah SU, Rao KV, Chaukar DA, et al. Extracellular 2'5'-
794 oligoadenylate synthetase 2 mediates T-cell receptor CD3-zeta chain down-regulation via caspase-3
795 activation in oral cancer. Immunology. 2016;147(2):251-64.
796 68. DeDiego ML, Nogales A, Martinez-Sobrido L, Topham DJ. Interferon-Induced Protein 44 Interacts
797 with Cellular FK506-Binding Protein 5, Negatively Regulates Host Antiviral Responses, and Supports Virus
798 Replication. mBio. 2019;10(4).
799 69. Zeng Y, Chen HQ, Zhang Z, Fan J, Li JZ, Zhou SM, et al. IFI44L as a novel epigenetic silencing tumor
800 suppressor promotes apoptosis through JAK/STAT1 pathway during lung carcinogenesis. Environmental
801 pollution. 2023;319:120943.
802 70. Cagnoni AJ, Giribaldi ML, Blidner AG, Cutine AM, Gatto SG, Morales RM, et al. Galectin-1 fosters
803 an immunosuppressive microenvironment in colorectal cancer by reprogramming CD8(+) regulatory T
804 cells. Proc Natl Acad Sci U S A. 2021;118(21).
805 71. Schlabach MR, Lin S, Collester ZR, Wrocklage C, Shenker S, Calnan C, et al. Rational design of a
806 SOCS1-edited tumor-infiltrating lymphocyte therapy using CRISPR/Cas9 screens. J Clin Invest.
807 2023;133(24).
808 72. Zhu C, Anderson AC, Schubart A, Xiong H, Imitola J, Khoury SJ, et al. The Tim-3 ligand galectin-9
809 negatively regulates T helper type 1 immunity. Nature immunology. 2005;6(12):1245-52.
810 73. Marti i Lindez AA, Dunand-Sauthier I, Conti M, Gobet F, Nunez N, Hannich JT, et al. Mitochondrial
811 arginase-2 is a cell-autonomous regulator of CD8+ T cell function and antitumor efficacy. JCI insight.
812 2019;4(24).
813 74. Lacher SB, Dorr J, de Almeida GP, Honninger J, Bayerl F, Hirschberger A, et al. PGE(2) limits
814 effector expansion of tumour-infiltrating stem-like CD8(+) T cells. Nature. 2024;629(8011):417-25.
815 75. Chen Q, Zhong G, Fang X, Lin C, Wang S, Li M. The multifaceted role of Sestrin 3 (SESN3) in
816 oxidative stress, inflammation and tumorigenesis. Biochim Biophys Acta Mol Cell Res.
817 2025;1872(5):119938.
818 76. Veliz K, Shen F, Shestova O, Shestov M, Shestov A, Sleiman S, et al. Deletion of CD38 enhances
819 CD19 chimeric antigen receptor T cell function. Mol Ther Oncol. 2024;32(2):200819.
820 77. Bishop AL, Lopez Del Amo V, Okamoto EM, Bodai Z, Komor AC, Gantz VM. Double-tap gene drive
821 uses iterative genome targeting to help overcome resistance alleles. Nat Commun. 2022;13(1):2595.

78. Moller L, Aird EJ, Schroder MS, Kobel L, Kissling L, van de Venn L, et al. Recursive Editing improves homology-directed repair through retargeting of undesired outcomes. Nat Commun. 2022;13(1):4550.
79. Anzalone AV, Randolph PB, Davis JR, Sousa AA, Koblan LW, Levy JM, et al. Search-and-replace genome editing without double-strand breaks or donor DNA. Nature. 2019;576(7785):149-57.
80. Witte IP, Lampe GD, Eitzinger S, Miller SM, Berrios KN, McElroy AN, et al. Programmable gene insertion in human cells with a laboratory-evolved CRISPR-associated transposase. Science. 2025;388(6748):eadt5199.
81. Yarnall MTN, Ioannidi EI, Schmitt-Ulms C, Krajeski RN, Lim J, Villiger L, et al. Drag-and-drop genome insertion of large sequences without double-strand DNA cleavage using CRISPR-directed integrases. Nat Biotechnol. 2023;41(4):500-12.
82. Suzuki K, Tsunekawa Y, Hernandez-Benitez R, Wu J, Zhu J, Kim EJ, et al. In vivo genome editing via CRISPR/Cas9 mediated homology-independent targeted integration. Nature. 2016;540(7631):144-9.
83. Haider S, Mussolino C. Fine-Tuning Homology-Directed Repair (HDR) for Precision Genome Editing: Current Strategies and Future Directions. International journal of molecular sciences. 2025;26(9).
84. Carusillo A, Haider S, Schafer R, Rhiel M, Turk D, Chmielewski KO, et al. A novel Cas9 fusion protein promotes targeted genome editing with reduced mutational burden in primary human cells. Nucleic Acids Res. 2023;51(9):4660-73.
85. Gagnon JD, Ansel KM. MicroRNA regulation of CD8(+) T cell responses. Noncoding RNA Investig. 2019;3.
86. Wheeler BD, Gagnon JD, Zhu WS, Munoz-Sandoval P, Wong SK, Simeonov DS, et al. The lncRNA Malat1 inhibits miR-15/16 to enhance cytotoxic T cell activation and memory cell formation. eLife. 2023;12.
87. Zhao F, Yang Z, Gu X, Feng L, Xu M, Zhang X. miR-92b-3p Regulates Cell Cycle and Apoptosis by Targeting CDKN1C, Thereby Affecting the Sensitivity of Colorectal Cancer Cells to Chemotherapeutic Drugs. Cancers (Basel). 2021;13(13).
88. Sasaki K, Kohanbash G, Hoji A, Ueda R, McDonald HA, Reinhart TA, et al. miR-17-92 expression in differentiated T cells - implications for cancer immunotherapy. Journal of translational medicine. 2010;8:17.
89. Steiner DF, Thomas MF, Hu JK, Yang Z, Babiarz JE, Allen CD, et al. MicroRNA-29 regulates T-box transcription factors and interferon-gamma production in helper T cells. Immunity. 2011;35(2):169-81.

860 **Figures**

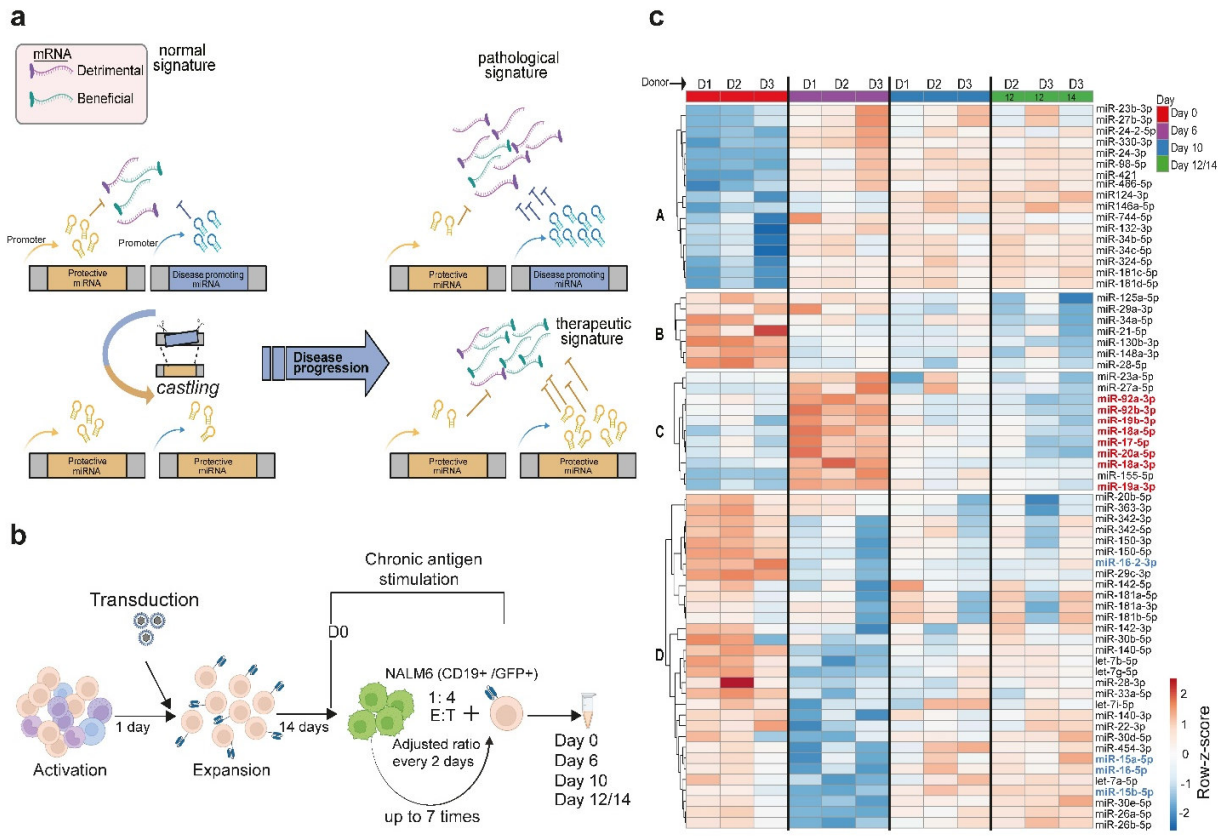

861

862 **Figure 1. Identification of candidate miRNA pairs for *castling*. a.** Schematic presentation of the miRNA
863 *castling* concept. **b.** Schematic presentation of the T cell manipulation flow. Upon thawing of peripheral
864 blood mononuclear cells (PBMC), T cells are activated and 24-hours later, transduced with a lentiviral
865 vector harboring the CD19-specific CAR construct. Following expansion (14 days), CD19+/GFP+ NALM6
866 tumor cells are added to the CAR T cells at a 1:4 effector-to-target (E:T) ratio (day 0) and chronic antigen
867 stimulation with the tumor cells continues for additional 12-14 days, adjusting the E:T ratio every two days.
868 The timepoints when the cells were harvested for subsequent miRNA/mRNA extraction and sequencing
869 are indicated. **c.** miRNA sequencing results. Heatmap depicts ln-transformed reads per million (RPM) after
870 row-based scaling values for 66 miRNAs, which were found to be differentially expressed (FDR < 0.05) on
871 day 6 as compared to day 0 (pre-stimulation), and which demonstrated medium or high abundance (mean

logCPM > 8). Letters A-D on the left side of the plot designate the types of miRNA expression profiles. Each group of three columns represents miRNA expression data obtained from cells originating from three independent T cell donors (D1, D2 and D3) and harvested at the indicated time points (day). Unit variance scaling was applied to rows, and clustered using Pearson correlation distance with average linkage. miRNAs selected for *castling* (miR-92b-3p and miR-17~92 cluster from profile C; miR-15/16 clusters from profile D) are highlighted in red or blue, respectively.

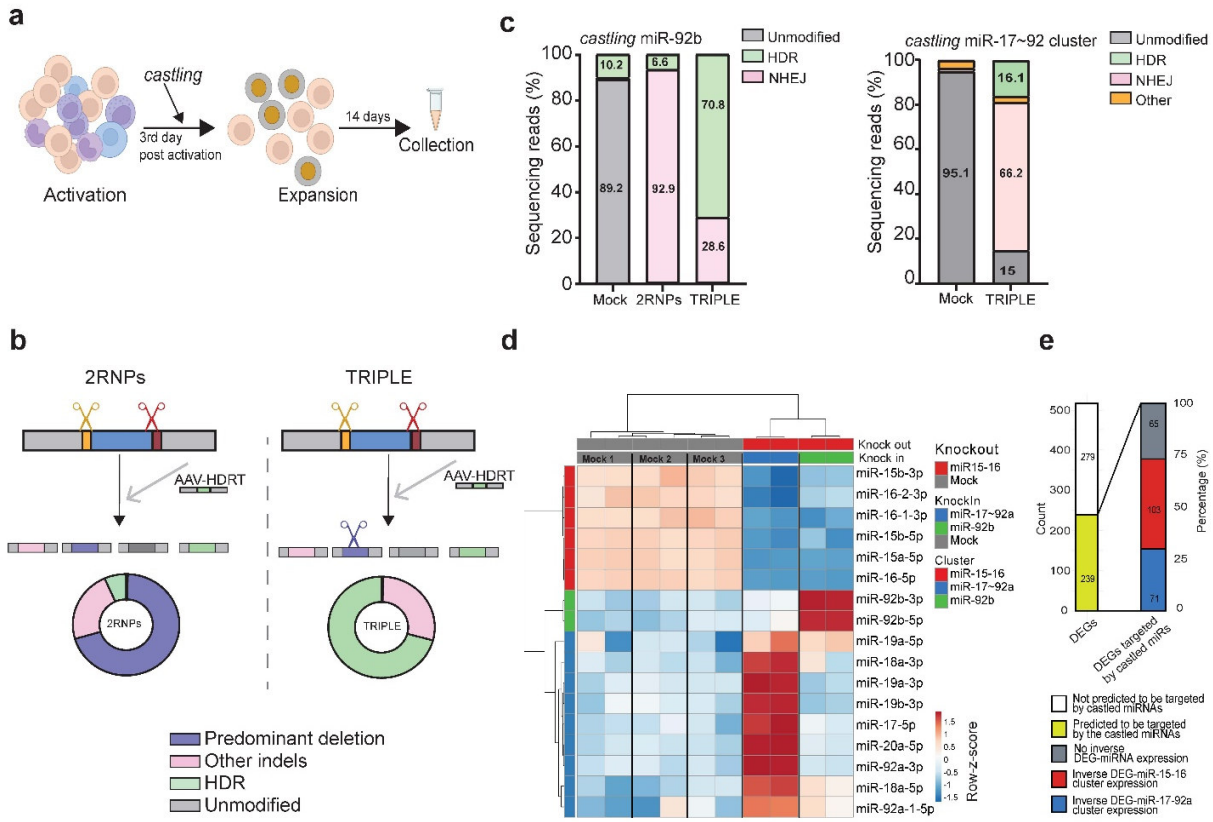

Figure 2. TRIPLE enables efficient miRNA *castling*. a. Schematic presentation of the experimental flow. PBMC are thawed and activated as indicated in figure 1a. Three days later, T cells are with the genome editing components for *castling*. Following 14 days of expansion, cells are harvested for subsequent analyisis. **b.** Schematic of the TRIPLE genome editing procedure. In conventional CRISPR–Cas9 editing, two ribonucleoprotein (RNP) complexes target sequences flanking the miRNA locus, resulting in excision of the

885 intervening region and generation of a predominant deletion allele (violet). In the TRIPLE approach, a third
886 RNP is simultaneously delivered to specifically target this predominant deletion junction, promoting
887 recurrent cleavage of the edited locus and thereby increasing the frequency of homology-directed repair
888 (HDR)–mediated insertion using the provided HDR template (HDRT). **c.** The bar graphs indicate the
889 integration efficiency of the miR-92b (left) and of the miR-17~92 cluster (right) at the miR-15a/16-1 locus
890 on chromosome 13, measured via short or long read sequencing, respectively, in the indicated sample.
891 The numbers within the bars indicate the percentage of sequencing reads of different types: unmodified
892 reads match the normal DNA sequence (grey); reads harboring indel mutations (pink) or precise miRNA
893 sequence integration (green) result from the activation of the non-homologous end-joining (NHEJ) or
894 homology directed repair (HDR) DNA repair pathways, respectively; other (orange) indicate sequences
895 that remained unclassified. **d.** Heatmap showing the scaled (unit variance) expression of the *castled*
896 miRNAs following miR-15/16 KO combined with KI of either miR-17~92 cluster or miR-92b. Rows and
897 columns were hierarchically clustered using Pearson correlation distance and average linkage. Each pair
898 of columns represents technical replicates of the indicated condition. All mock samples are electroporated
899 without genome editing components and either left non-transduced (Mock 1) or transduced with the
900 respective AAV-HDRT (Mock2: mir92b; Mock 3: miR-17~92 cluster). **e.** Bar graph summarizing the number
901 of differentially expressed genes (DEGs) identified via bulk RNA-seq in the indicated sample relative to
902 mock controls (FDR < 0.05). DEGs are classified as either not predicted (white) or predicted (yellow) to be
903 targeted by the *castled* miRNAs. The latter are further subdivided into transcripts with expression not
904 inversely correlated with the *castled* miRNA expression (grey), or inversely correlated with miR-15/16 (red)
905 or with miR-17~92 cluster members (blue).
906

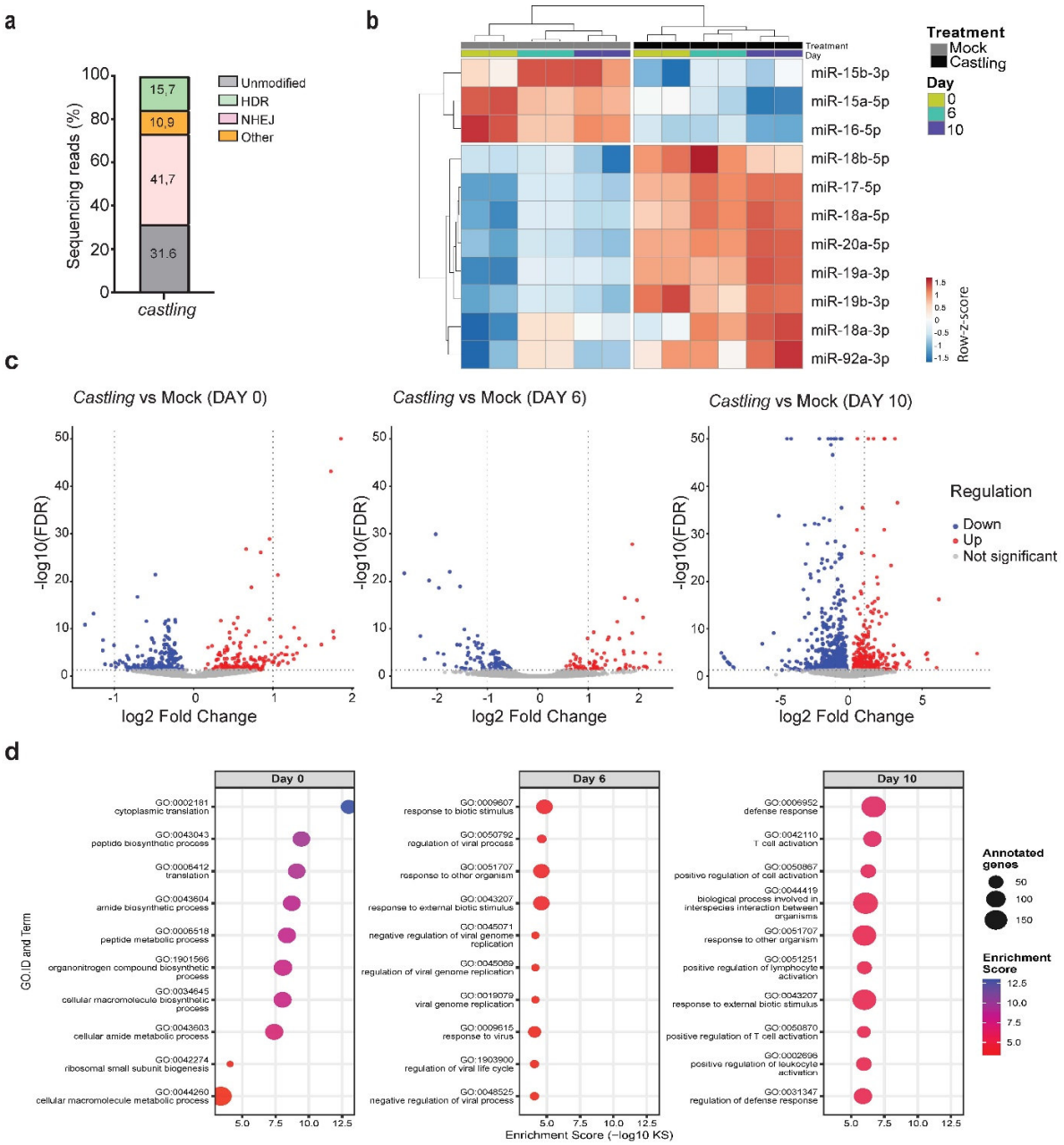

Figure 3. Effect of miR-17~92/miR-15a/16-1 *castling* in CAR T cells subjected to chronic antigen stimulation. a. Bar graph showing genome editing efficiency for the *castling* of the miR-17~92 cluster into the miR-15a/16-1 locus, measured via long read amplicon sequencing. Reads are classified as indicated in figure 2c. **b.** Heatmap showing the expression level of the *castled* miRNA measured via small RNA sequencing in the indicated samples. Each group of two columns corresponds to two technical replicates

913 of the indicated sample. **c.** Volcano plots (upper) depicting differential gene expression between *castled*
914 and mock-transfected CAR T cells at the indicated time points, shown as log2 fold change (x-axis) versus
915 −log10 false discovery rate (FDR; y-axis). The top 10 enriched Gene Ontology (GO) biological process terms,
916 identified among differentially expressed genes at each time point using a Kolmogorov–Smirnov (KS)
917 enrichment test, are show in the lower panels.

918

919 **Tables**

920 **Table 1: The role of microRNAs (miRNAs) selected for castling in T cell function.**

miRNA	Function in T cells	References
miR15/16 cluster	Restricts the proliferation of antigen specific T cells; restricts the survival and early differentiation of CD8+ memory T cells.	(45, 85, 86)
miR-92b-3p	Promotes proliferation	(44, 87)
miR17~92 cluster	Promotes proliferation, IFN γ production (critical for Th1 response and CD4+ T cell antitumor response); prevents activation induced death of CD4+ T cells	(43, 88, 89)

921

922

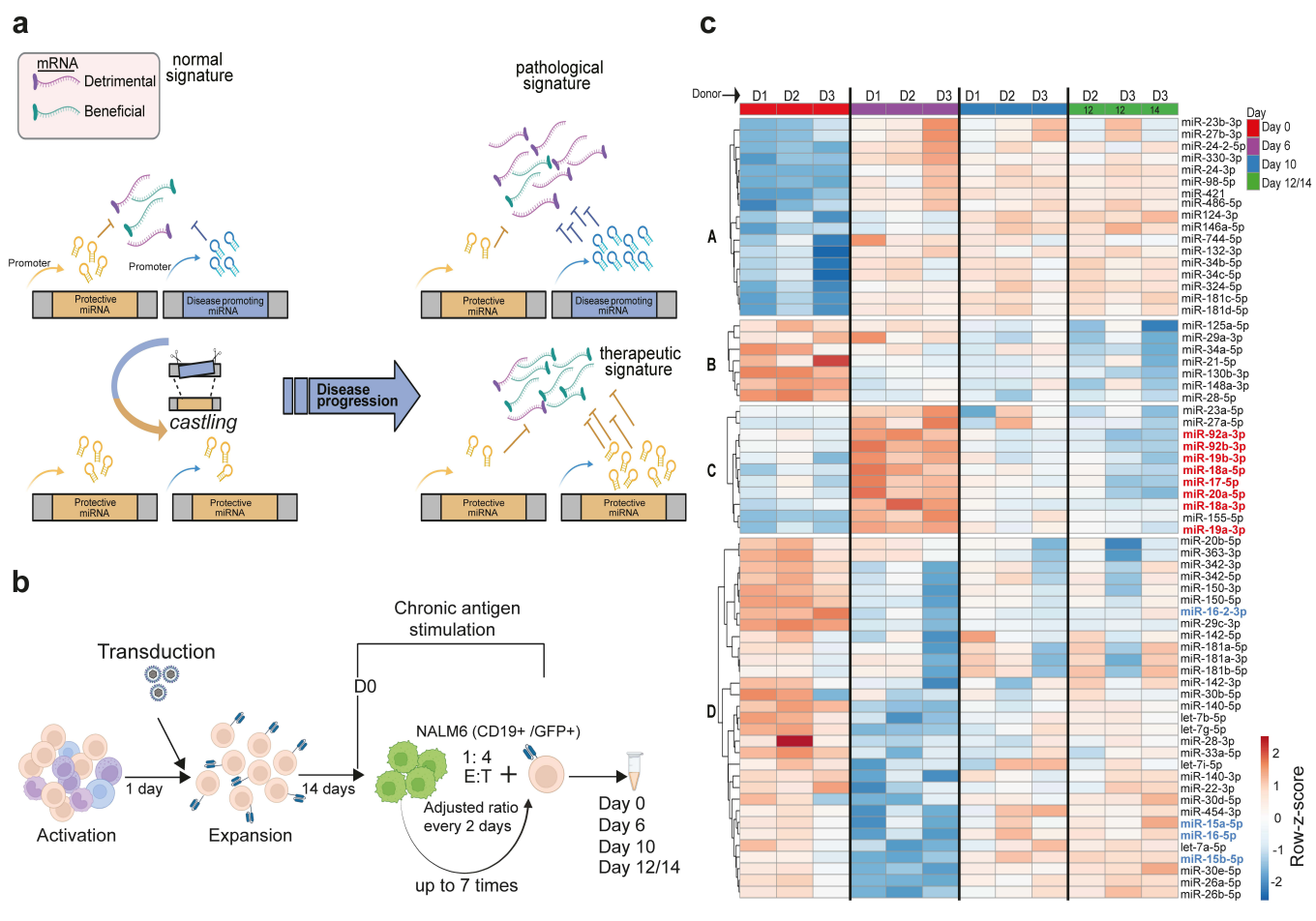

Antony et al. Figure 1

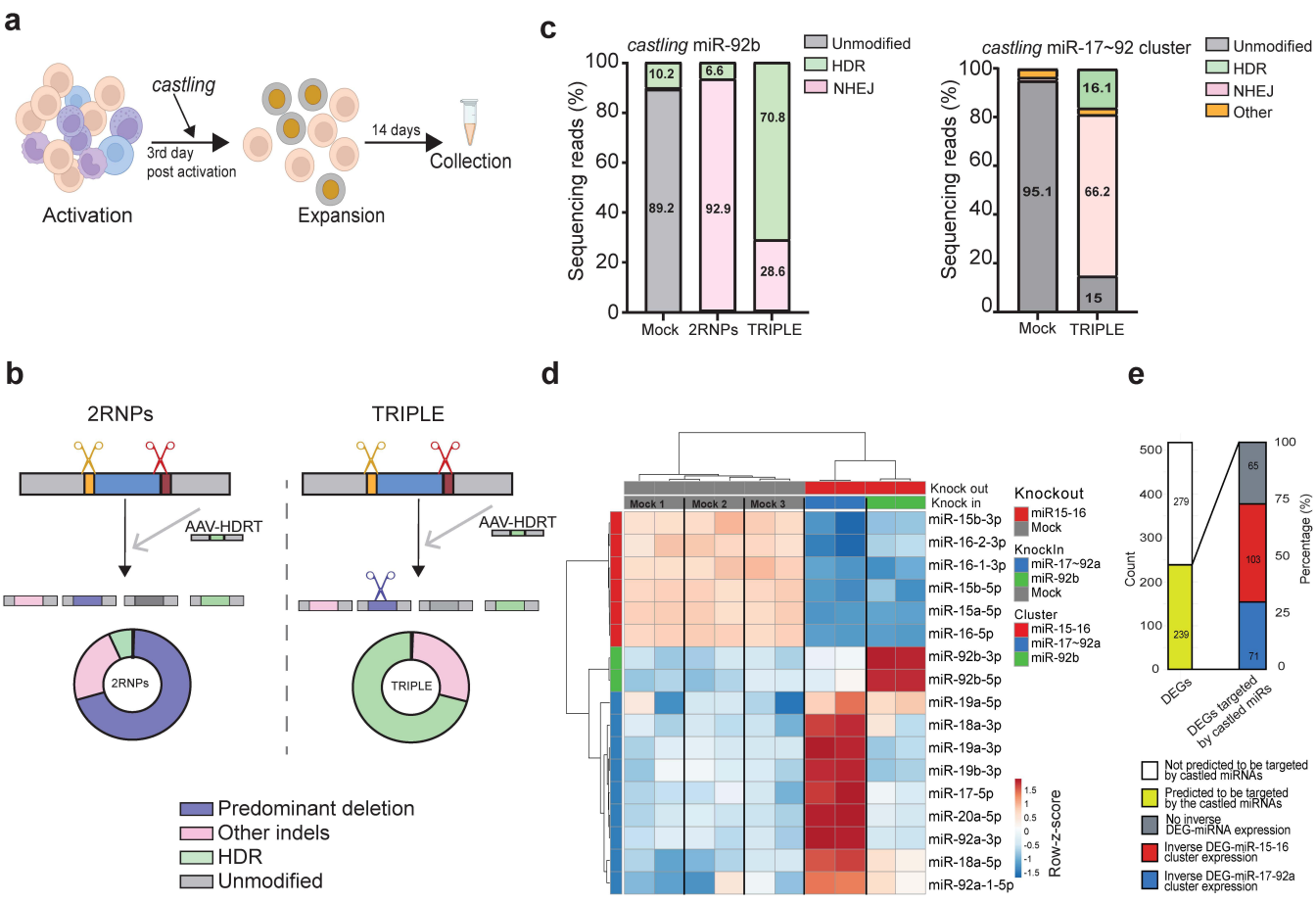

Antony et al. Figure 2

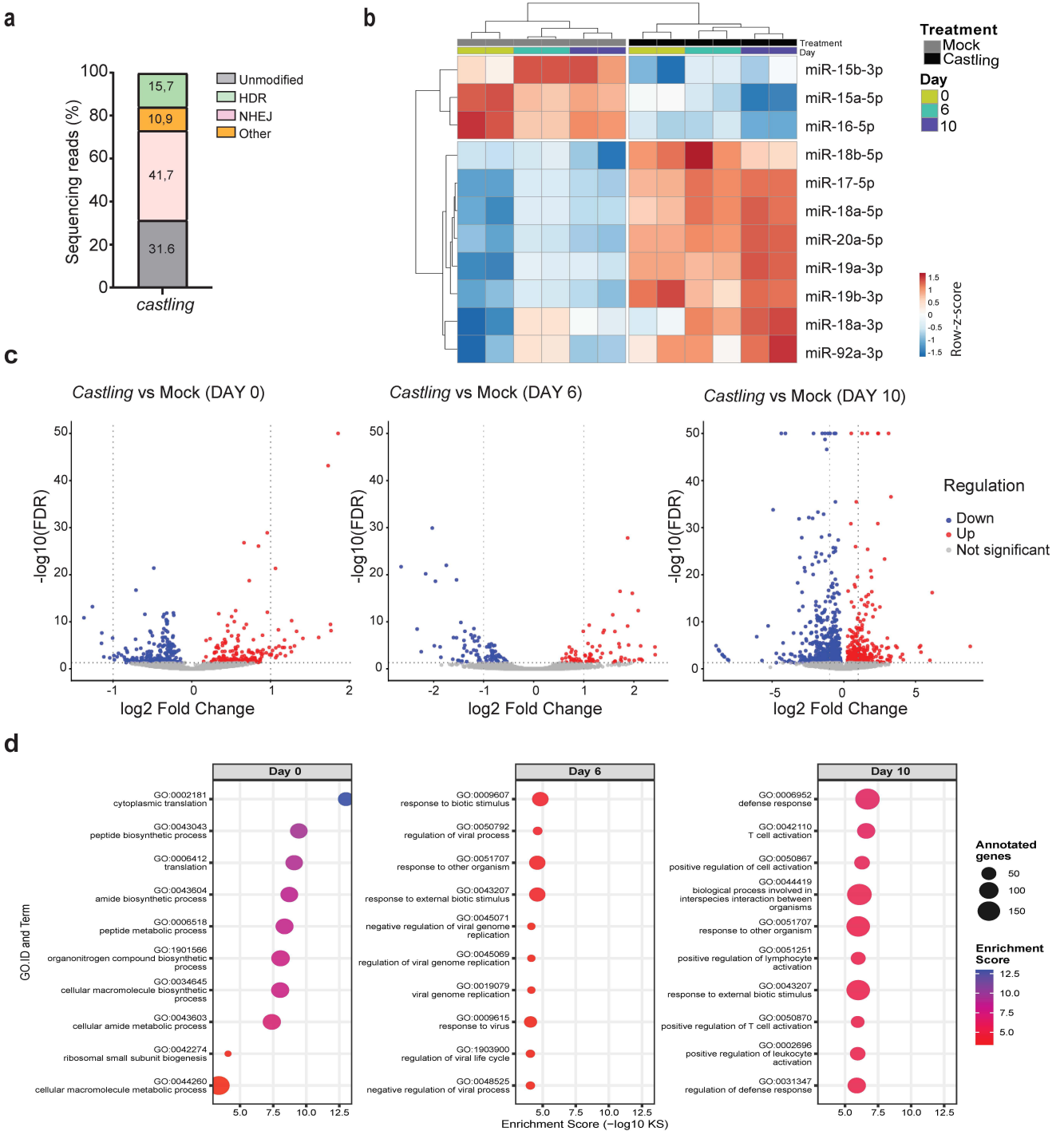

Antony et al. Figure 3